www.sciencemag.org/cgi/content/full/science.aaf2807/DC1

Supplementary Materials for

Epigenetic stability of exhausted T cells limits durability of reinvigoration by PD-1 blockade

Kristen E. Pauken, Morgan A. Sammons, Pamela M. Odorizzi, Sasikanth Manne, Jernej Godec, Omar Khan, Adam M. Drake, Zeyu Chen, Debattama Sen, Makoto Kurachi, R. Anthony Barnitz, Caroline Bartman, Bertram Bengsch, Alexander C. Huang, Jason M. Schenkel, Golnaz Vahedi, W. Nicholas Haining, Shelley L. Berger, E. John Wherry*

*Corresponding author. Email: wherry@mail.med.upenn.edu

Published 27 October 2016 on *Science* First Release
DOI: 10.1126/science.aaf2807

This PDF file includes:

Other Supplementary Materials for this manuscript includes the following:
(available at www.sciencemag.org/cgi/content/full/science.aaf2807/DC1)

Table S1. List of genes significantly differentially expressed following anti-PDL1 treatment.
Table S2. GSEA reports showing GO and KEGG pathways identified following anti-PD-L1 treatment.
Table S3. Gene list and GSEA report for effector genes.
Table S4. List of genes identified using Leading Edge Metagene analysis and overlaps between cell types.
Table S5. Differentially expressed genes one day or 18-29 weeks after cessation of anti-PD-L1 treatment in the RNA-seq data set.
Table S6. GO term enrichments in the RNA-seq data set.
Table S7. List of ATAC-seq peaks annotated with nearest genes corresponding to distinct co-clusters.
Table S8. GO terms associated with ATAC-seq peaks gained exclusive to each cell type.
Table S9. Full list of transcription factor binding motifs present in open chromatin regions gained or lost in TEX following anti-PD-L1 treatment.

Table S10. Full list of transcription factors predicted to have uniquely enriched binding in OCRs in TN, TEFF, TMEM, TEX, or anti-PD-L1-treated TEX.
Table S11. Association of differentially expressed genes with transcription factors predicted to have altered activity in ATAC-seq data set.
Table S12. Transcription factors predicted to regulate differentially expressed genes following anti-PD-L1.

Materials and Methods

Mice, infections, and antibody treatment

Five to six week old female C57BL/6 and B6-Ly5.2CR (B6 mice expressing Ly5.1) were purchased from Charles River (NCI strains). C57BL/6 P14 mice were bred to B6-Ly5.2CR mice to generate P14 Ly5.1^{+} mice as described (*32*). LCMV strains (Armstrong (Arm) and clone 13) were propagated and titers were determined as described (*32*). B6 mice were infected intraperitoneally (i.p.) with 2x10^{5} PFU LCMV Arm or intravenously (i.v.) with 4x10^{6} PFU LCMV clone 13 to establish acute or persistent infection, respectively. For all clone 13 infections, CD4 T cells were depleted by i.p. injection of 200 μg of anti-CD4 (clone GK1.5, Bio X Cell) on days $^{-}$1 and $^{+}$1 p.i. with LCMV clone 13. Anti-PD-L1 (clone 10F.9G2, Bio X Cell) or an isotype control antibody (Rat IgG2b, Bio X Cell) was administered i.p. starting between day 22-25 p.i., 200 μg/injection for five injections every third day for 5 total treatments as described (*5*). For some experiments vehicle (PBS) was injected as a control. For experiments where IL-7 was administered *in vivo*, the cytokine was complexed to anti-IL-7 to increase stability. For these experiments, IL-7/anti-IL-7 immune complexes (i.c.) were prepared as described (*33*). Briefly, 1.5 μg of recombinant human IL-7 (NCI Preclinical Repository or Biolegend) and 7.5 μg of anti-human/anti-mouse IL-7 (clone m25, provided by Charlie Surh) per mouse per injection were mixed and allowed to complex for 30 min prior to diluting with PBS for injection. Complexes were administered i.p. simultaneously with anti-PD-L1 (every third day for 5 injections). All mice were maintained under specific pathogen free conditions at the University of Pennsylvania, and all protocols were approved by the Institutional Animal Care and Use Committee.

Lymphocyte isolation and adoptive transfer

For experiments where P14 cells were monitored, P14 cells were isolated from the peripheral blood of P14 transgenic mice using histopaque gradients, and P14 cells (500 for clone 13 experiments, and 500-2000 for Arm experiments) were adoptively transferred i.v. into 5-6 weeks old recipient B6 mice at least one day prior to infection. Similar results were obtained when comparing P14 cells to endogenous D^bGP33^+ and D^bGP276^+ cells (Figure S4), and previous reports have shown that the number of P14 cells transferred for clone 13 experiments (500) did not impact viral load (*32, 34*). For experiments where T_{MEM}, T_{EX}, or anti-PD-L1-treated T_{EX} were adoptively transferred, CD8 T cells were isolated one day post the antibody treatment period from spleens, and were enriched using CD8 T cell EasySep negative selection kits (Stem Cell Technologies) according to the manufacturer's instructions. Numbers were normalized between groups based on D^bGP33 tetramer staining prior to i.v. adoptive transfer into antigen free recipient mice. LCMV immune mice (day 30^+ p.i.) were used as antigen free recipients so endogenous LCMV-specific memory could eliminate any transferred virus as described (*18*). For experiments testing antigen-independent persistence, recipient mice were immune to LCMV Arm (day 30^+ pi). For rechallenge experiments, recipient mice had previously cleared low dose (200 PFU) infection with LCMV clone 13 V35A lacking the GP33 epitope as described (*12*). V35A immune mice were used for recall experiments to prevent direct competition with endogenous D^bGP33-specific memory CD8 T cells.

Flow cytometry

MHC class I peptide tetramers (D^bGP276 and D^bGP33) were made as described (*32*) or obtained from the NIH tetramer core. Antibodies were purchased from eBioscience, BD, Biolegend, Life Technologies, R&D Systems and AbD Serotec, and included CD8, CD4, B220, CD45.1, CD45.2, CD44, CD122, CD127, PD-1, 2B4, Tim-3, Lag-3, Ki-67, granzyme B, IFNγ, TNFα, and phospho-STAT5. Single cell suspensions were stained with Live/Dead Aqua (Life Technologies) according to the manufacturer's instructions prior to staining for surface antigens. Intracellular staining for Ki-67 and granzyme B was performed using the eBioscience Foxp3 fixation/permeabilization kit according to manufacturer's instructions (eBioscience). Intracellular staining for IFNγ and TNFα was performed using the BD cytofix/cytoperm kit according to manufacturer's instructions (BD) following a 5 hour *in vitro* restimulation with 0.2 μg/ml gp33-41 peptide (KAVYNFATM, GenScript) in the presence of brefeldin A and monensin (BD). For phosho-STAT5 detection, splenocytes were rested for 1-2 hours at 37°C prior to stimulation. Cells were stimulated for 30 minutes with 10 ng/ml recombinant murine IL-7 or IL-15 (Peprotech). Cells were then fixed with paraformaldehyde for 15 minutes at 37°C, washed once, and immediately resuspended in Phospho Perm Buffer III (BD) and incubated for 30 minutes on ice. Cells were subsequently washed and stained according to manufacturer's instructions. Cells were collected on an LSR II flow cytometer (BD), and data were analyzed using FlowJo software (Tree Star). Sorting was conducted on a FACSAria (BD), and post-sort purities were obtained to determine sort quality.

Gene expression by microarray and RNA-seq

For transcriptional profiling by microarray, CD8 T cells from spleens 1-2 days after the final treatment (after receiving 5 total treatments as described above) were enriched using magnetic beads (CD8 negative selection kit, Stem Cell Technologies) and D^bGP276^+ CD8 T cells were sorted on a FACSAria (BD). Four independent experiments were performed for each treatment group with 10-12 mice pooled per group per experiment. RNA was isolated with TRIzol (Life Technologies) according to manufacturer's instructions. RNA was processed, amplified, labeled, and hybridized to Affymetrix GeneChip MoGene 2.0 ST microarrays at the University of Pennsylvania Microarray Facility. Microarray data were processed and analyzed as previously described (*29*). The heat map module in Gene Pattern was used to identify and display differentially expressed genes. Gene set enrichment analyses and leading edge metagene analyses were performed as described (*11*). Metagenes for anti-PD-L1 were identified using the microarray data set comparing anti-PD-L1 to control T_{EX}. Metagenes for T_{EFF} (Day 8 post-LCMV Arm infection), T_{MEM} (Day 30 post-LCMV Arm infection), and T_{EX} (Day 30 post-LCMV clone 13 infection) cells were generated by comparing to naïve T cells using previously published transcriptional profiles (*29*). Details of the metagene composition and comparisons can be found in Table S4. To generate the effector gene list shown in Figure 1C, we started with the top 300 genes up-regulated at Day 6 post Arm compared to naïve in (*29*). We then removed genes that had GO membership for six of the major cell cycle terms (cell cycle, mitosis, spindle, DNA replication, mitotic cell cycle, and cell cycle). This list is shown in Table S3.

For transcriptional profiling by RNA-seq, CD8 T cells from spleens were enriched using magnetic beads (CD8 negative selection kit, Stem Cell Technologies) and

P14 cells were sorted on a FACSAria (BD). P14 cells were sorted either 1 day post final treatment (with 5 doses of anti-PD-L1 or control as described above; three independent experiments for control (5-7 mice each pooled), four independent experiments for anti-PD-L1 (5-6 mice each pooled)), or long-term (two independent experiments, at 18 (5 control-treated and 7 anti-PD-L1-treated mice pooled) and 29 weeks (13 control-treated and 12 anti-PD-L1-treated mice pooled)) after the final treatment. Naïve $CD8^+$ T cells were sorted from pooled spleens from 2-3 uninfected C57BL/6 mice from two independent experiments. Cells were lysed and frozen in buffer RLT plus (RNeasy Plus Lysis Buffer, Qiagen) with 1% 2-mercaptoethanol (Sigma). Total RNA from sorted cells was extracted using the Applied Biosystems Arcturus PicoPure RNA isolation kit. Double stranded cDNA was generated using the Clontech SMRT-seq v4 method and was fragmented using the Covaris S220 in microTubes. Indexed Illumina-compatible sequencing libraries were generated from fragmented cDNA using the NEBNext Ultra II methodology. Libraries were quantified using Kapa Library QC kit for Illumina, pooled, and sequenced on an Illumina NextSeq 500 for 75 cycles (single end). Sequenced libraries were aligned to the mm10 reference genome using STAR and gene expression from RefSeq genes was quantified using Cufflinks and reported as FPKM values.

Epigenetic profiling by ATAC-seq

CD8 T cells were enriched using magnetic beads (CD8 negative selection kit, Stem Cell Technologies) and P14 CD8 T cells (day 8 p.i. Arm (5 spleens per experiment pooled), day 33 p.i. Arm (12-13 spleens per experiment pooled), day 35 p.i. clone 13 (15 spleens per experiment for control-treated pooled, 7 mice per experiment for anti-PD-L1-

treated pooled)) or naïve CD8 T cells (from 2-3 spleens pooled) were sorted on a FACSAria (BD). Control- and anti-PD-L1-treated T_{EX} cells were sorted one day after the final treatment (5 total treatments, every third day) as described above. Two independent experiments per condition were performed. ATAC-seq was performed as described (*20*). Briefly, nuclei were isolated from 50,000-150,000 sorted cells per replicate using a solution of 10 mM Tris-HCl, 10 mM NaCl, 3 mM $MgCl_2$, and 0.1% IGEPAL CA-630. Immediately following nuclei isolation, the transposition reaction was conducted using Tn5 transposase and TD buffer (Illumina) for 45 minutes at 37^{o}C. Transposed DNA fragments were purified using a Qiagen MinElute Kit, barcoded with dual indexes (Illumina Nextera) and PCR amplified using NEBNext High Fidelity 2x PCR master mix (New England Labs). The size distribution and molarity of the sequencing library were determined by using an Agilent Bioanalyzer and KAPA quantitative RT-PCR (KAPA Biosystems). Sequencing was performed using a high output, 150 cycle kit with V2 chemistry on a NextSeq 500 (Illumina). Paired-end reads were mapped to the mm10 reference genome using Bowtie2. Only concordantly mapped pairs were kept for further analysis. Peak calling was performed using MACS v1.4 to identify areas of sequence tag enrichment. BedTools was used to find common intersection between identified peaks (1bp minimum overlap) and to create a merged peak list. ATAC-seq tag enrichment, DNA motif analysis across the merged peak list, and GO term assessment were computed using HOMER (homer.salk.edu). Principal component analysis, spectral co-clustering, and hierarchical clustering were performed using scipy, matplotlab, and scikit-learn. REVIGO was used to identify unique GO terms across different cell types. The list of

peaks was filtered for some downstream analysis to remove peaks that had low enrichment across all five cell types (third quartile).

Transcription Factor Footprinting and Network analysis

To build the integrated transcriptional network based on the unique epigenetic landscape of T_{EX} (Figure 4D), Wellington bootstrap (*35*) was first used to identify transcription factor (TF) binding motifs enriched in either control- or anti-PD-L-treated T_{EX} in all OCRs compared to the other cell types probed by computing 20 sets of differential footprints for all ordered pairs of the 5 cell types (T_N, T_{EFF}, T_{MEM}, T_{EX}, anti-PD-L1-treated T_{EX}). To analyze motif frequencies in differential footprints, a motif search was done within these footprint coordinates using annotatePeaks.pl script from HOMER (*36*) and relative motif frequencies were calculated as described in (*35*). A matrix was generated and motif scores were displayed as a heat map (Figure 4B) using the ClassNeighbors module of GenePattern (*37*) to show cell-type specific TFs.

Significantly enriched TF binding motifs were subsequently validated to be included in the downstream network. TFs that were not detectable transcriptionally in the RNA-seq and/or TFs that had minimal evidence of binding to their consensus sequence with TF footprint analysis were excluded. For TF footprint validation, average profiles of the Tn5 cuts within a 200 bp window around different TF motifs were estimated and plotted using Wellington dnase_average_footprinting.py (*38*). A network was then built with these validated TFs and the differentially expressed genes in T_{EX} cells following anti-PD-L1 treatment from the microarray data set. Genes were included that had a LFC$\geq$0.3. Lines connecting a TF with a target gene were based on that gene having a

consensus binding motif for that TF in the region. The full list of TFs and target genes is available in Table S11.

To validate TFs identified in this integrated network analysis correlating the epigenetic landscape and transcriptional changes, we constructed a second network using the differentially expressed genes from the microarray following anti-PD-L1 treatment (LFC≥0.3 up or down, $p<0.05$) and used PSCAN to identify the TFs predicted to contain consensus binding motifs in the promoter regions of those genes (Table S12). The enrichment for each TF for the differentially expressed genes was plotted as a heat map (Figure S18). To test the prediction that anti-PD-L1 caused a re-engagement of effector-like circuitry in T_{EX}, we determined genes near all OCRs in T_{EFF} or T_{EX} cells that contained consensus binding motifs for TFs identified in the integrated network analysis (Figure 4D) and selected additional TFs of interest including T-bet, Eomes, *Prdm1* (Blimp1), and Runx1-3. We excluded genes near OCRs for which there was no transcriptional data in the microarray. The percentage of genes changed following anti-PD-L1 that contained membership in the list for the overlap between T_{EFF} and T_{EX} or T_{EX} alone was then calculated, and the percent difference in the overlap compared to T_{EX} alone was plotted.

Statistical analysis

Statistics for flow cytometry and viral load data were analyzed using GraphPad Prism software. For comparisons between two independent conditions when only two conditions were being compared, significance was determined using unpaired Student's t tests. Paired Student's t tests were used when samples from the same mouse were being

compared at two different time points as indicated in the Figure Legends. One way ANOVA tests were used when more than two groups were being compared. We first tested for normality using the D'Agostino and Pearson normality test. If all groups were determined to be normally distributed, a parametric one way ANOVA was performed, and post-test analyses of groups of interest were performed using Bonferroni's multiple comparison test. If not all groups were determined to be normally distributed, a non-parametric ANOVA (Kruskal-Wallis test) was performed, and post-test analyses of groups of interest were performed using Dunn's multiple test comparisons. P values for the ANOVA are indicated in blue next to the Y axis in each figure, and the p values for post-tests between indicated pairs are in black. P values were considered significant if less than 0.05. Asterisks used to indicate significance correspond with: $p<0.05$*, $p<0.01$**, $p<0.001$***.

Fig. S1

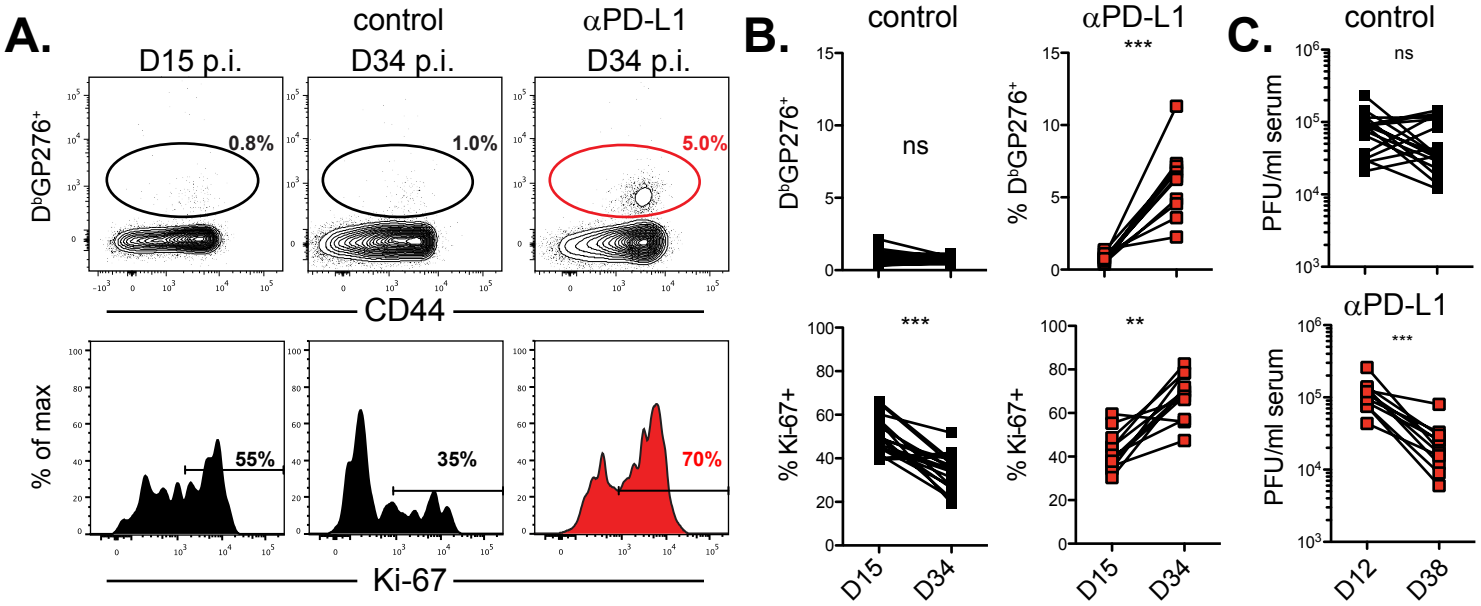

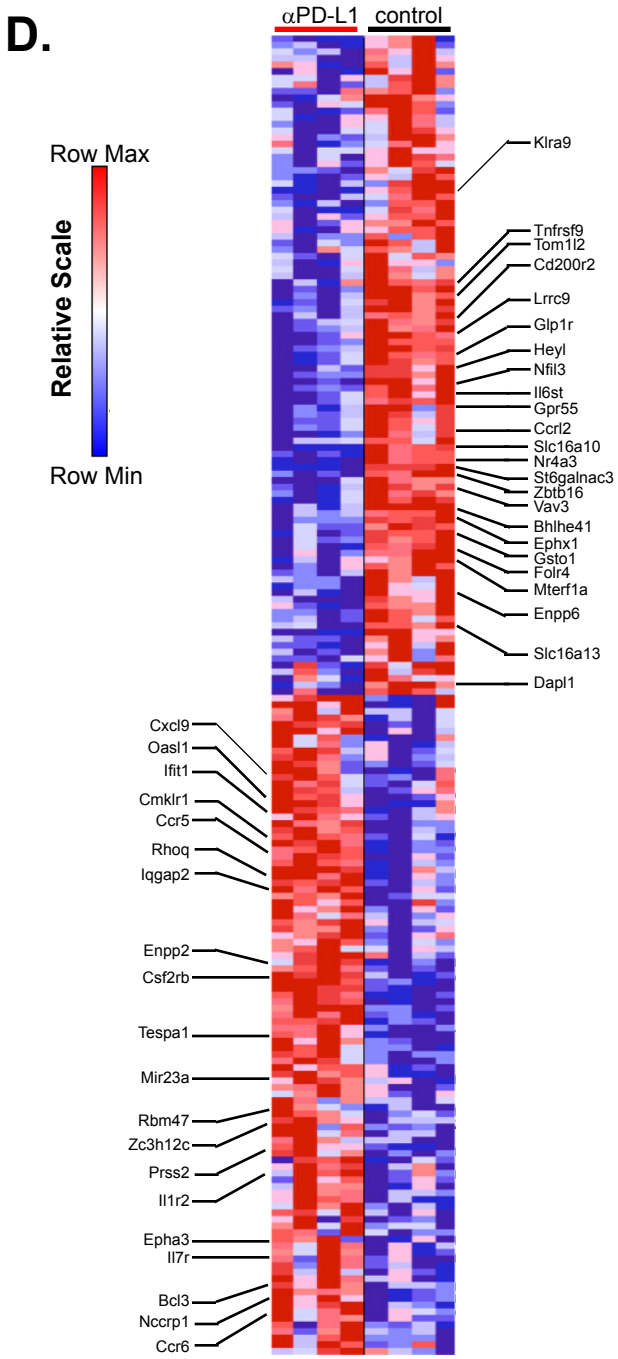

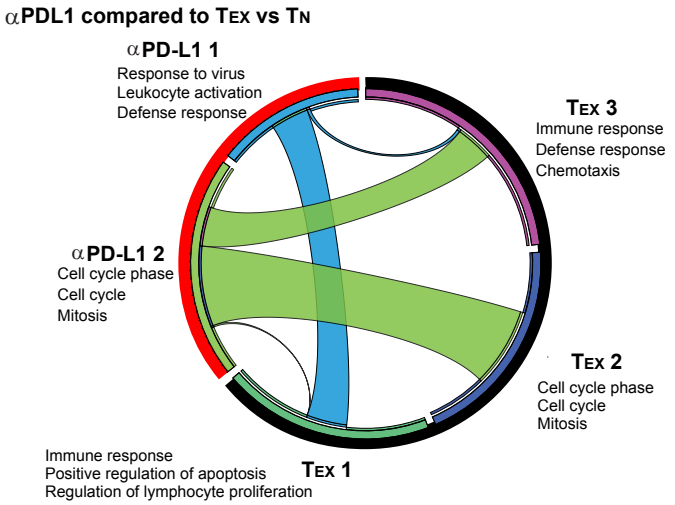

F.

LEM #:	Description	P value	FDR
TEFF vs TN 1	Immune response Response to wounding Chemotaxis	1.4E-9 1.3E-7 3E-6	2.2E-6 2.2E-4 4.9E-3
TEFF vs TN 2	Cell cycle phase Cell cycle Mitosis	6.4E-74 8.7E-74 1.3E-60	5.3E-71 1.3E-70 1.9E-57
TMEM vs TN 1	Immune Response Cellular defense response Reg. of Protein Kinase cascade	5.3E-8 3.3E-7 9.5E-4	8.4E-5 5.2E-4 1.5E0
TMEM vs TN 2	Leukocyte adhesion	1.9E-2	2.6E1
TMEM vs TN 3	Immune Response Neg. Reg. of Apoptosis Reg. of Leukocyte Act.	4.9E-14 2.7E-9 3.1E-9	8.1E-11 4.5E-6 5.2E-6
TEX vs TN 1	Immune response Positive reg. of apoptosis Reg. of lymphocyte proliferation	9.1E-19 5.7E-9 9.6E-7	1.5E-15 9.3E-6 4.3E-4
TEX vs TN 2	Cell cycle phase Cell cycle Mitosis	3.1E-64 5.2E-61 1.4E-51	4.7E-61 8E-58 2.1E-48
TEX vs TN 3	Immune response Defense Response Chemotaxis	9.6E-9 1.3E-7 6.1E-4	1.6E-5 2.1E-4 9.9E-1
αPD-L1 vs TEX 1	Response to virus Leukocyte activation Defense response	7.2E-19 4.1E-4 1.33E-6	1.1E-15 6.2E-1 2.0E-3
αPD-L1 vs TEX 2	Cell cycle phase Cell cycle Mitosis	6.8E-51 1.4E-47 2E-44	1E-47 2.2E-44 3E-41

Fig. S1. Impact of anti-PD-L1 treatment on the transcriptional profile of T_{EX}. (A) Representative flow cytometry plots gated on $CD8^+$ cells (top) or histograms gated on D^bGP276 tetramer$^+$ cells (bottom) on PBMCs isolated from mice before (day 15 p.i.) or after (day 34 p.i.) treatment with control or anti-PD-L1 antibody. (B) Quantification of (A) showing frequency of D^bGP276 tetramer$^+$ cells of $CD8^+$ cells (top) and Ki-67^+ of D^bGP276 tetramer$^+$ cells (bottom) in PBMC. (C) Viral load (plaque forming units/ml) in the serum pre- (day 12) and post- (day 38) treatment from mice shown in (B). Lines connecting dots in (B) and (C) indicate data from the same mouse pre- and post-treatment. Asterisks indicating significance determined by paired t tests between groups are **$p<0.01$ and ***$p<0.001$. Data are representative of at least three independent experiments with at least 5 mice per group. (D) Row normalized heat map showing top genes significantly differentially expressed based on fold change in microarray data. Selected genes are indicated. Full list of genes with fold changes and p values available in Table S1. (E) Circos plot showing overlap in metagenes identified in control- versus anti-PD-L1 treated T_{EX} compared to metagenes in T_{EX} versus T_N. Transcriptional data for T_{EX} versus T_N obtained from (*29*). (F) P value and FDR q values for metagenes comparing T_{EFF}, T_{MEM}, or T_{EX} to T_N from (*29*), and anti-PD-L1-treated T_{EX} to control-treated T_{EX} from Figure 1. Details of metagene gene membership and overlaps can be found in Table S4.

Fig. S2

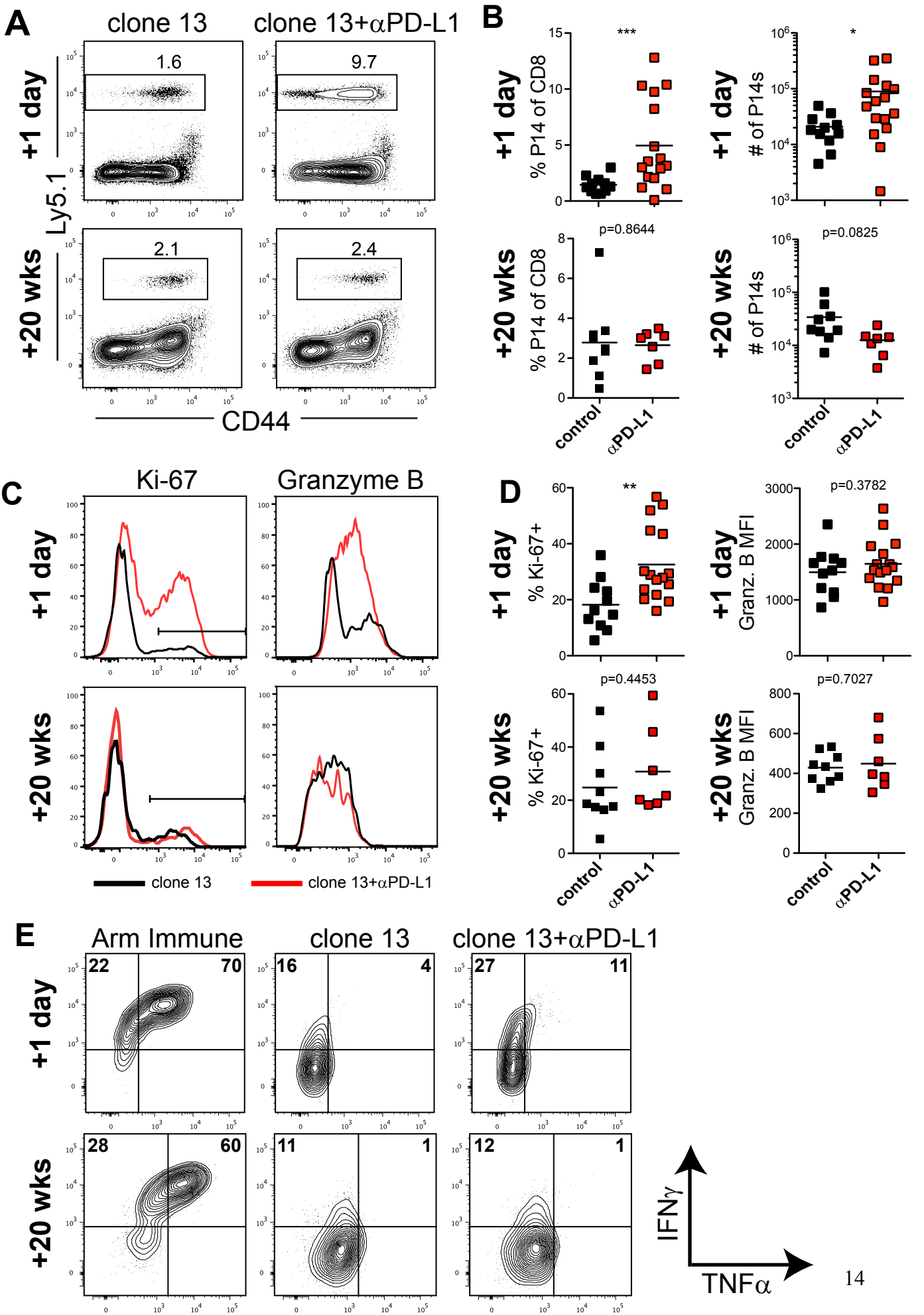
A
clone 13
clone 13+αPD-L1
+1 day
+20 wks
Ly5.1
CD44
1.6
9.7
2.1
2.4
B
+1 day
+20 wks
% P14 of CD8
# of P14s
***
*
p=0.8644
p=0.0825
control
αPD-L1
C
Ki-67
Granzyme B
clone 13
clone 13+αPD-L1
D
% Ki-67+
Granz. B MFI
**
p=0.3782
p=0.4453
p=0.7027
E
Arm Immune
22
70
16
4
27
11
28
60
11
1
12
1
IFNγ
TNFα

Fig. S2. Virus-specific CD8 T cells re-exhaust after cessation of anti-PD-L1 treatment. (A) Representative flow cytometry plots gated on $CD8^+$ T cells showing P14s ($Ly5.1^+$ cells) in the spleen one day or 20 weeks after cessation of anti-PD-L1 treatment. (B) Quantification of P14 frequency (left) and number (right) in the spleen from mice shown in (A). (C) Flow cytometry histograms of Ki-67 (left) and granzyme B (right) in the spleen. (D) Quantification of (C). (E) Representative flow cytometry plots gated on P14 cells following *ex vivo* stimulation with gp33-41 peptide, showing IFNγ and TNFα production quantified in Figure 1I. The mice shown in (A)-(E) correspond to the mice shown in Figure 1H and 1I. The $^+$1 day time point is combined from two representative experiments and the $^+$20 week time point is from one representative experiment. Data are representative of at least two independent experiments with at least 4 mice per group per experiment. Asterisks indicating significance determined by unpaired t tests between groups are * $p<0.05$, ** $p<0.01$, and *** $p<0.001$.

Fig. S3

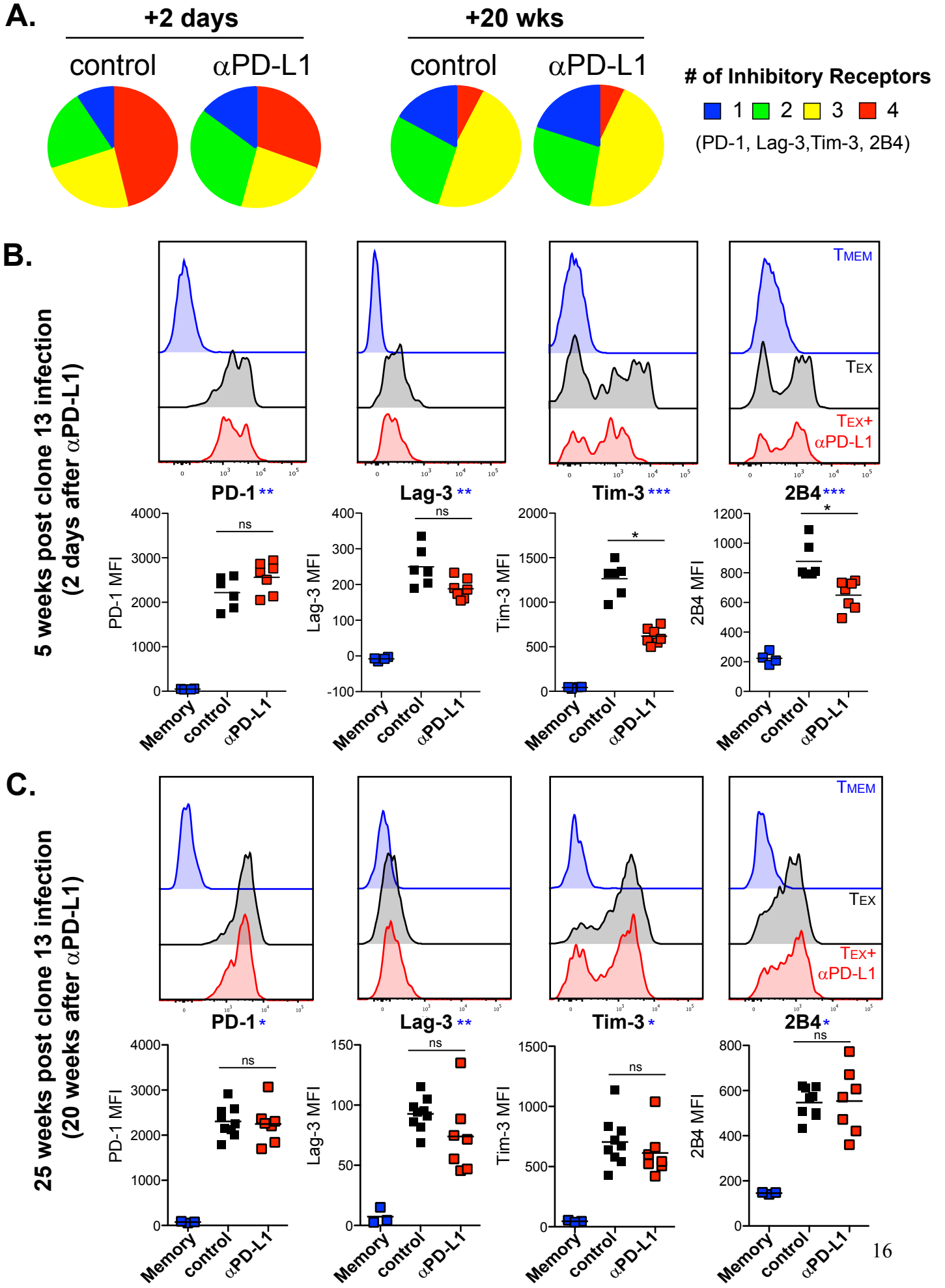
A.
+2 days
+20 wks
control
αPD-L1
control
αPD-L1
# of Inhibitory Receptors
1 2 3 4
(PD-1, Lag-3,Tim-3, 2B4)
B.
5 weeks post clone 13 infection
(2 days after αPD-L1)
TMEM
TEX
TEX+
αPD-L1
PD-1 **
Lag-3 **
Tim-3 ***
2B4 ***
PD-1 MFI
Lag-3 MFI
Tim-3 MFI
2B4 MFI
ns
*
Memory
control
αPD-L1
C.
25 weeks post clone 13 infection
(20 weeks after αPD-L1)
PD-1 *
Lag-3 **
Tim-3 *
2B4 *

Fig. S3. Inhibitory receptor expression following anti-PD-L1 treatment. (A) Co-expression of inhibitory receptors on P14 cells in the spleen 2 days (left) or 20 weeks (right) after cessation of treatment. Representative histograms (top) and quantification of geometric MFIs from multiple mice (bottom) showing PD-1, Lag-3, Tim-3, and 2B4 (B) two days or (C) 20 weeks after anti-PD-L1 treatment during clone 13 infection. Arm immune mice were day 30^{+} p.i. Gated on P14 cells. Data are representative of two independent experiments with at least three mice per Arm immune group and at least five mice per clone 13 group. Statistical significance was determined using non-parametric one-way ANOVA. Asterisk indicating significance between groups is * $p<0.05$, ** $p<0.01$, and *** $p<0.001$. Blue asterisks indicate ANOVA p values, black asterisks indicate post-test p values.

Fig. S4

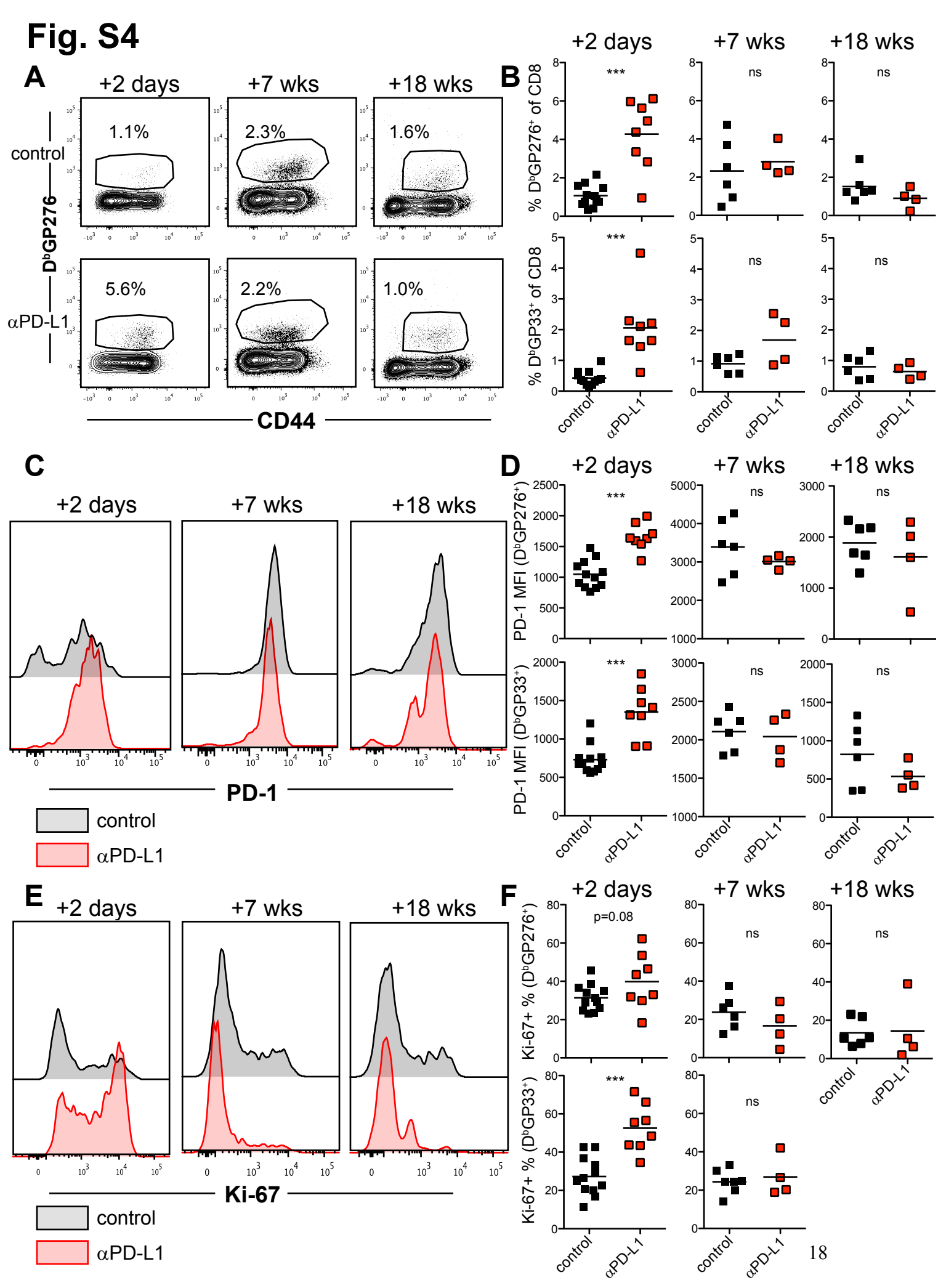
A
+2 days
+7 wks
+18 wks
control
αPD-L1
DbGP276
1.1%
2.3%
1.6%
5.6%
2.2%
1.0%
CD44
B
+2 days
+7 wks
+18 wks
% DbGP276+ of CD8
% DbGP33+ of CD8
***
ns
control
αPD-L1
C
+2 days
+7 wks
+18 wks
PD-1
control
αPD-L1
D
+2 days
+7 wks
+18 wks
PD-1 MFI (DbGP276+)
PD-1 MFI (DbGP33+)
***
ns
control
αPD-L1
E
+2 days
+7 wks
+18 wks
Ki-67
control
αPD-L1
F
+2 days
+7 wks
+18 wks
Ki-67+ % (DbGP276+)
Ki-67+ % (DbGP33+)
p=0.08
***
ns
control
αPD-L1

Fig. S4. Re-invigoration of endogenous virus-specific CD8 T cells wanes over time when antigen remains high. Monitoring of endogenous virus-specific CD8 T cell responses at 2 days (in peripheral blood), 7 weeks (spleen), or 18 weeks (spleen) post-anti-PD-L1 treatment. (A) Representative plots showing D^bGP276 tetramer and CD44. (B) Quantification of the frequency of D^bGP276^+ (top) and D^bGP33^+ (bottom) of the total $CD8^+$ population. (C) Representative histograms of PD-1 expression, gated on D^bGP276^+ cells. (D) Quantification of geometric MFI of PD-1, gated on D^bGP276^+ cells (top) or D^bGP33^+ cells (bottom). (E) Representative histograms showing Ki-67 expression. (F) Quantification of the frequency of $Ki\text{-}67^+$ D^bGP276^+ (top) or D^bGP33^+ (bottom). Data are representative of two independent experiments with at least four mice per group. Asterisks indicating significance determined by unpaired t tests between groups are ***$p<0.001$.

Fig. S5

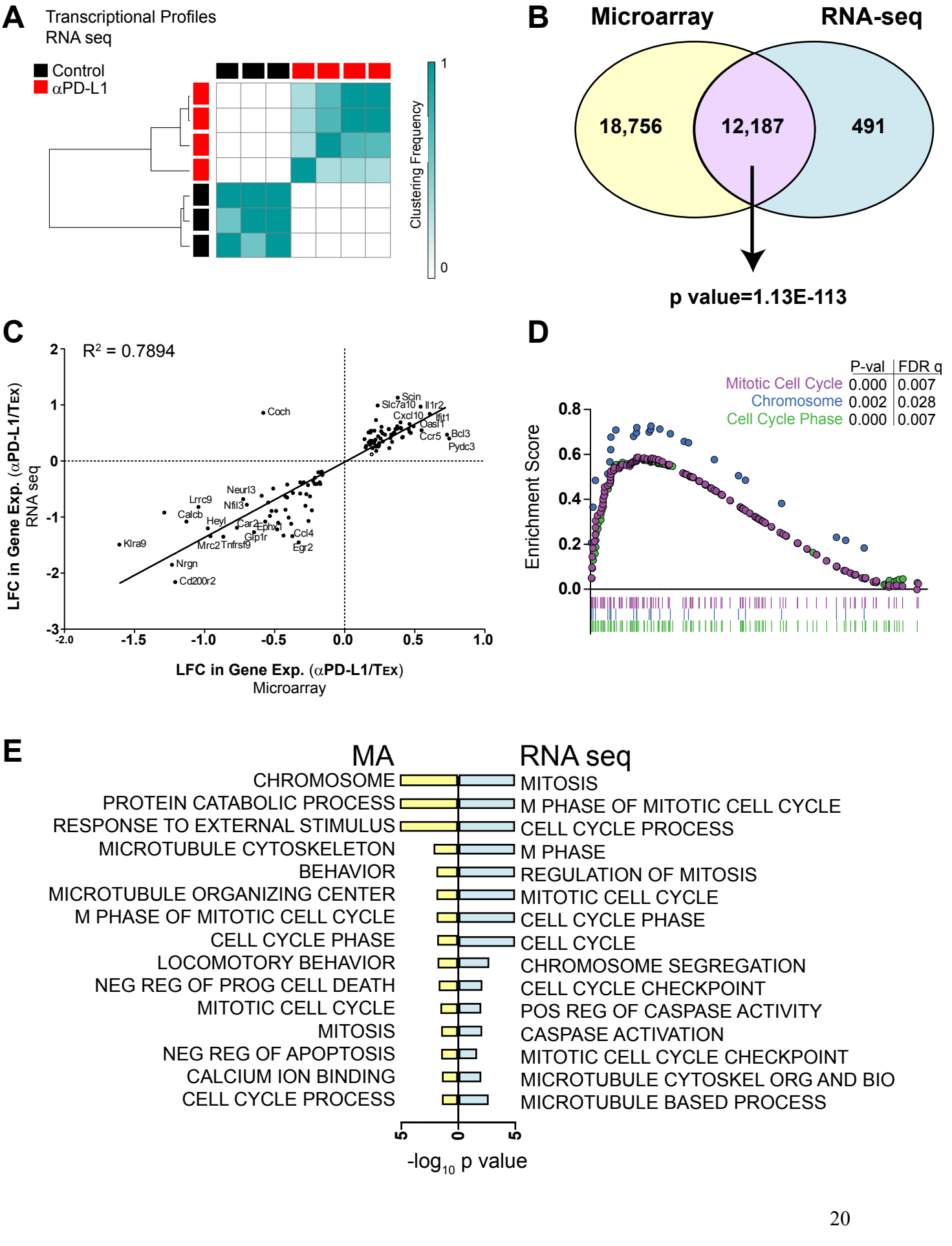
A
Transcriptional Profiles
RNA seq
Control
αPD-L1
Clustering Frequency
1
0
B
Microarray
RNA-seq
18,756
12,187
491
p value=1.13E-113
C
R² = 0.7894
LFC in Gene Exp. (αPD-L1/Tex) RNA seq
LFC in Gene Exp. (αPD-L1/Tex) Microarray
Coch
Scin
Slc7a10
Il1r2
Cxcl10
Ifit1
Oasl1
Ccr5
Bcl3
Pydc3
Neurl3
Lrrc9
Nfil3
Calcb
Heyl
Car2
Ephx1
Gfp1r
Ccl4
Egr2
Klra9
Mrc2
Tnfrsf9
Nrgn
Cd200r2
D
P-val
FDR q
Mitotic Cell Cycle 0.000 0.007
Chromosome 0.002 0.028
Cell Cycle Phase 0.000 0.007
Enrichment Score
E
MA
RNA seq
CHROMOSOME
PROTEIN CATABOLIC PROCESS
RESPONSE TO EXTERNAL STIMULUS
MICROTUBULE CYTOSKELETON
BEHAVIOR
MICROTUBULE ORGANIZING CENTER
M PHASE OF MITOTIC CELL CYCLE
CELL CYCLE PHASE
LOCOMOTORY BEHAVIOR
NEG REG OF PROG CELL DEATH
MITOTIC CELL CYCLE
MITOSIS
NEG REG OF APOPTOSIS
CALCIUM ION BINDING
CELL CYCLE PROCESS
MITOSIS
M PHASE OF MITOTIC CELL CYCLE
CELL CYCLE PROCESS
M PHASE
REGULATION OF MITOSIS
MITOTIC CELL CYCLE
CELL CYCLE PHASE
CELL CYCLE
CHROMOSOME SEGREGATION
CELL CYCLE CHECKPOINT
POS REG OF CASPASE ACTIVITY
CASPASE ACTIVATION
MITOTIC CELL CYCLE CHECKPOINT
MICROTUBULE CYTOSKEL ORG AND BIO
MICROTUBULE BASED PROCESS
-log10 p value

Fig. S5. Comparison of transcriptional profiles of control and anti-PD-L1-treated T_{EX} cells generated by microarray or RNA-seq. (A) Consensus hierarchical clustering of genes from the RNA-seq by variance (by 1-Pearson correlation) between T_{EX} from control or anti-PD-L1-treated mice isolated 1 day after the two week treatment period. (B) Overlap in genes assessed in microarray and RNA-seq data sets from mice 1 day after treatment. (C) Comparison of LFCs of differentially expressed genes ($p<0.05$) after anti-PD-L1 treatment in the microarray and RNA-seq data sets. LFC=log fold change. Complete list of differentially expressed genes are available in Table S1 for the microarray and Table S5 for the RNA seq. (D) GSEAs of representative significantly enriched GO terms. Complete list of GO terms for RNA-seq available in Table S6. (E) Top 15 significantly enriched GO terms in anti-PD-L1 treated T_{EX} compared to control T_{EX} in the microarray (left) and RNA-seq (right). Complete list of GO terms available in Table S2 for the microarray and Table S6 for the RNA seq.

Fig. S6

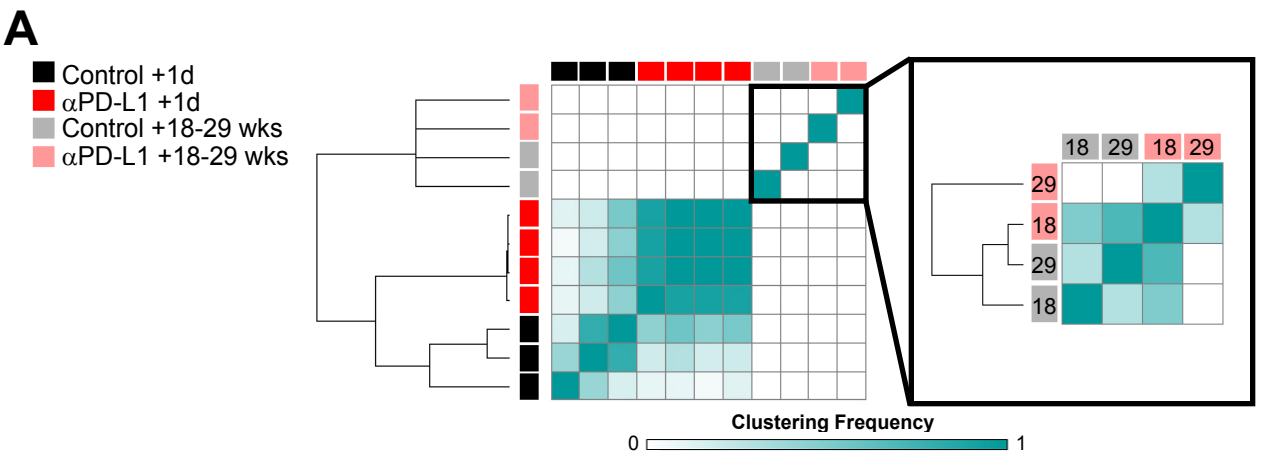

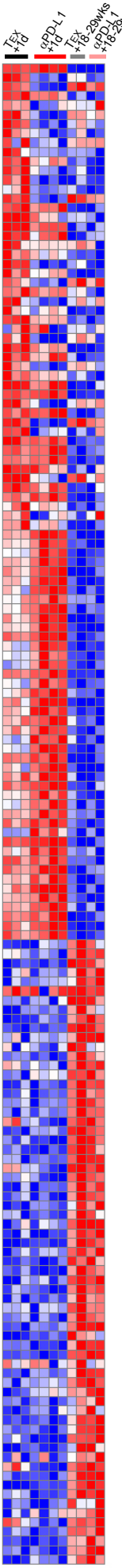

C

Comparison	Total genes	Sig (p≤0.05)	LFC≥0.58	LFC≤-0.58
TEX vs αPD-L1 (+1d)	12678	239	54	29
TEX vs αPD-L1 (+18-29wks)	12678	31	6	3
TEX (+1d vs 18-29wks)	12678	1008	168	346
αPD-L1 (+1d vs 18-29wks)	12678	1336	334	411

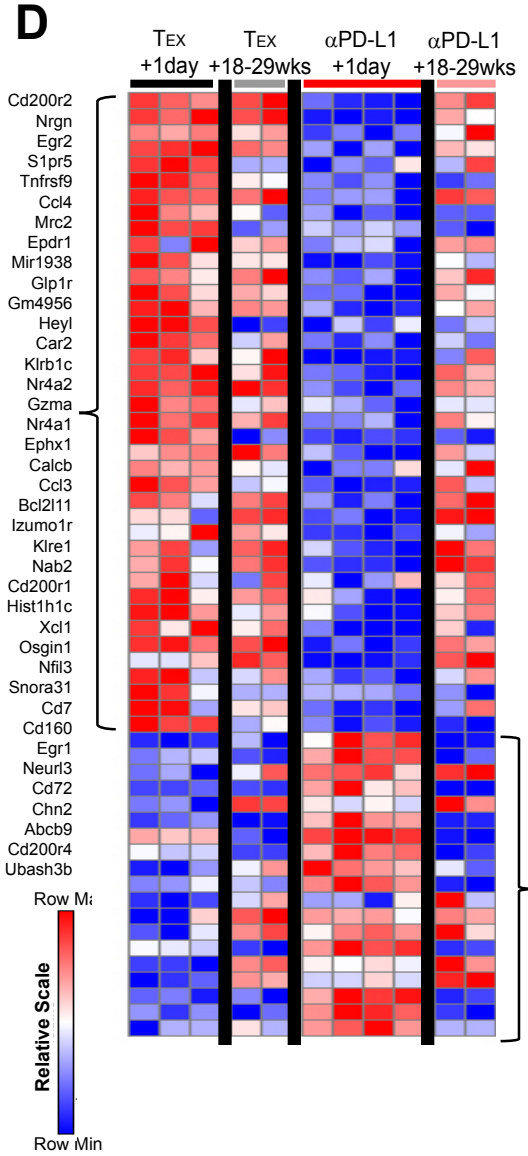

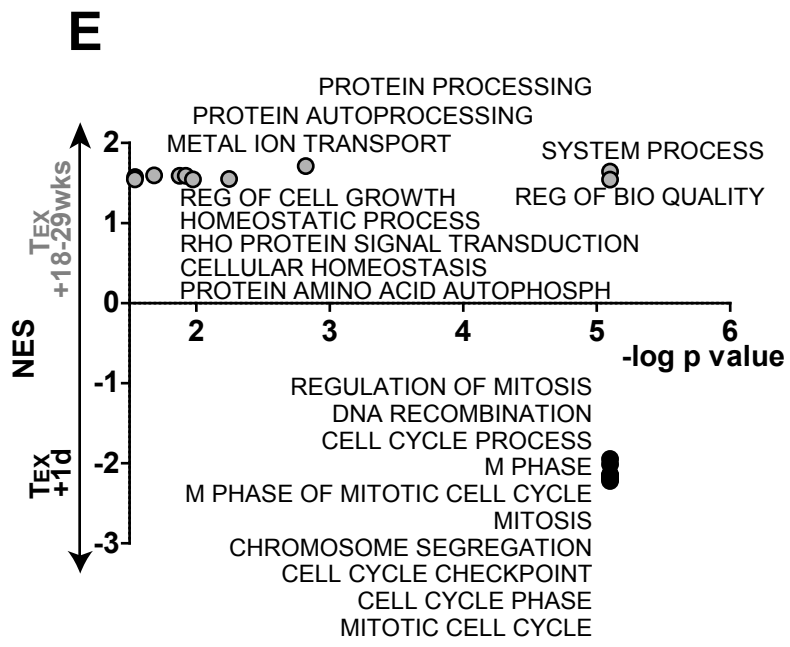

Fig. S6. Temporal changes in the transcriptional profiles of T_{EX} with or without anti-PD-L1 treatment using RNA-seq. (A) Consensus hierarchical clustering of genes from the RNA-seq by variance (by 1-Pearson correlation) between T_{EX} from control or anti-PD-L1-treated mice 1 day or 18-29 weeks after cessation of treatment. Clustering of all four groups shown to the left, pairwise comparison of control and anti-PD-L1-treated T_{EX} 18-29 weeks post treatment shown boxed to the right. (B) Heat map of class neighbor analysis, showing the top genes differentially expressed in control or anti-PD-L1-treated T_{EX} 1 day or 18-29 weeks after cessation of anti-PD-L1 treatment. Full list of genes available in Table S5. (C) Table comparing the number of significantly changed genes in pairwise comparisons between the indicated treatments and time points. Full list of genes available in Table S5. (D) Heat map of RNA-seq showing top differentially expressed genes following anti-PD-L1 treatment one day after treatment, and corresponding expression of those genes 18-29 weeks after treatment. (E) Top GO terms associated with control T_{EX} 1 day or 18-29 weeks after treatment. Full list of pairwise comparisons for short-term versus long-term, anti-PD-L1 versus control-treated T_{EX} available in Table S6.

Fig. S7

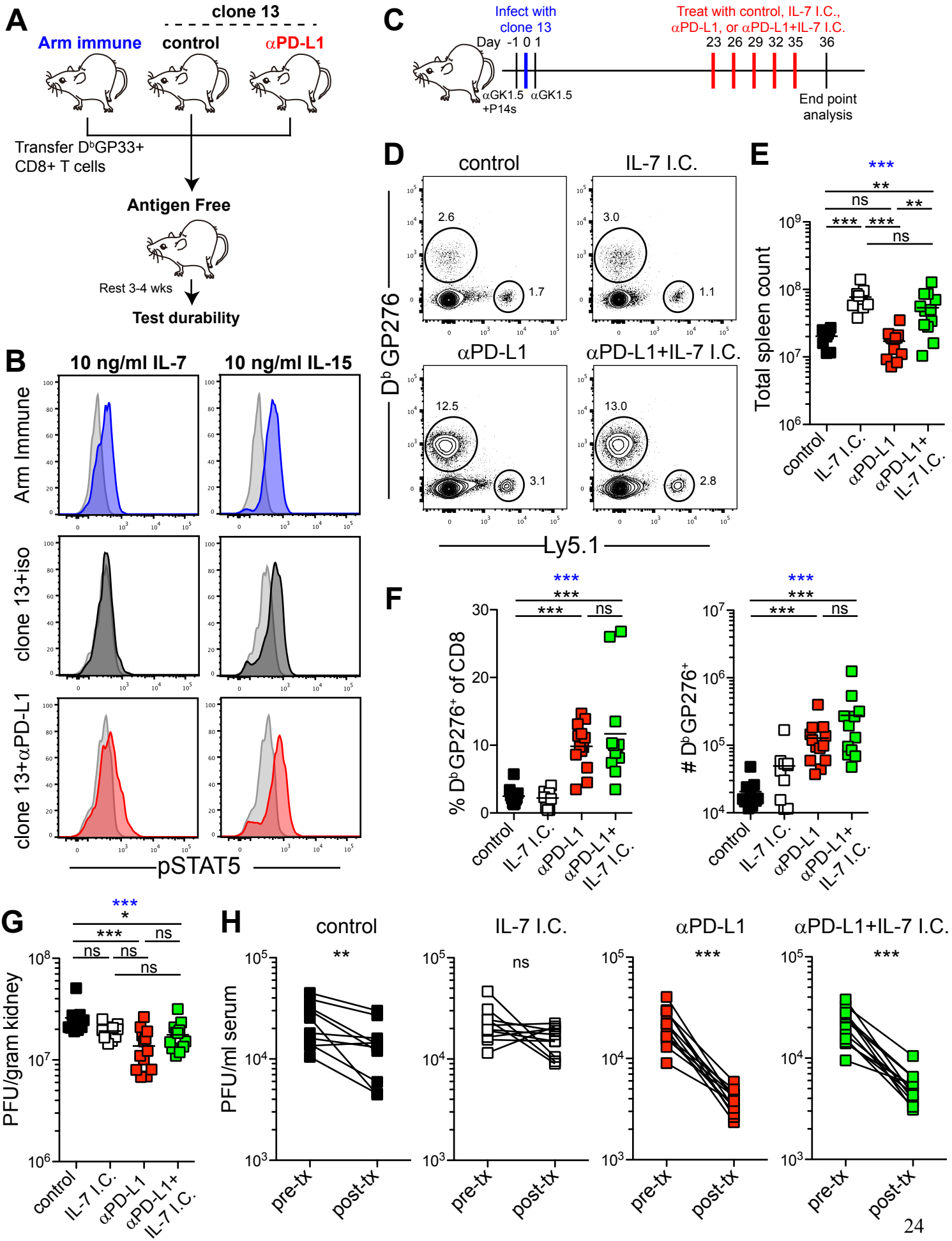
A
clone 13
Arm immune
control
αPD-L1
Transfer DbGP33+
CD8+ T cells
Antigen Free
Rest 3-4 wks
Test durability
B
10 ng/ml IL-7
10 ng/ml IL-15
Arm Immune
clone 13+iso
clone 13+αPD-L1
pSTAT5
C
Infect with
clone 13
Day -1 0 1
αGK1.5 αGK1.5
+P14s
Treat with control, IL-7 I.C.,
αPD-L1, or αPD-L1+IL-7 I.C.
23 26 29 32 35
36
End point
analysis
D
control
IL-7 I.C.
αPD-L1
αPD-L1+IL-7 I.C.
DbGP276
Ly5.1
2.6
1.7
3.0
1.1
12.5
3.1
13.0
2.8
E
Total spleen count
control
IL-7 I.C.
αPD-L1
αPD-L1+
IL-7 I.C.
F
% DbGP276+ of CD8
# DbGP276+
G
PFU/gram kidney
H
PFU/ml serum
pre-tx
post-tx

Fig. S7. Combination treatment with IL-7 i.c. and anti-PD-L1 augments virus-specific CD8 T cell responses *in vivo*. (A) Experimental design for Figure 2A and 2B. (B) Representative flow cytometry histograms gated on P14 cells from spleens isolated at day 39 p.i. following *ex vivo* stimulation with IL-7 or IL-15 for 30 minutes. Shaded grey histograms are unstimulated controls, colored histograms are stimulated with cytokine. Quantification for multiple mice shown in Figure 2F. (C) Schematic for experimental design for combination therapy with anti-PD-L1 and IL-7 i.c. (D) Representative flow cytometry plots gated on $CD8^+$ T cells showing D^bGP276^+ cells and P14 cells ($Ly5.1^+$). Numbers next to gates indicate frequency of each population of $CD8^+$ parent population. (E) Total number of viable cells in spleens following treatment with control, IL-7 i.c. anti-PD-L1, or both anti-PD-L1 and IL-7 i.c. Since data was normally distributed, significance was determined using a parametric one-way ANOVA and Bonferroni's multiple comparison test to compare groups. (F) Frequency (left) and number (right) of D^bGP276^+ CD8 T cells from mice shown in (E). (G) Viral load in the kidney following treatment for the mice in (E). For (F) and (G), significance was determined using a non-parametric one-way ANOVA (Kruskal-Wallis test) and Dunn's multiple test comparison to compare groups. For (E)-(G), blue asterisks indicate ANOVA p values, black asterisks indicate post-test p values. (H) Viral load in the serum pre- and post-treatment for the mice in (E). Lines connect serial measurements from the same mouse. Significance determined using paired Student's t tests for each treatment group. Data from (D)-(H) are combined from two independent experiments with at least four mice per group. These data correspond with the mice shown in Figure 2G and 2H. Asterisks indicating significance are * $p<0.05$, ** $p<0.01$, and *** $p<0.001$.

Fig. S8

A

	Total Paired Reads	Number Aligned	% Aligned	# of Peaks (MACS v1.4)
TN-1	21,580,793	19,895,761	92.19	47,245
TN-2	37,179,087	34,405,396	92.54	52,242
TEFF-1	52,854,827	47,732,769	90.31	64,351
TEFF-2	51,028,317	46,145,040	90.43	60,124
TMEM-1	61,364,436	42,757,634	69.68	58,448
TMEM-2	60,666,170	55,654,432	91.74	58,676
TEX-1	48,137,474	42,639,858	88.58	39,225
TEX-2	66,496,181	60,252,069	90.61	59,910
αPDL1-1	49,545,282	44,790,886	90.40	55,036
αPDL1-2	59,567,799	53,608,743	90.00	56,564

B Normalized ATAC peak enrichment

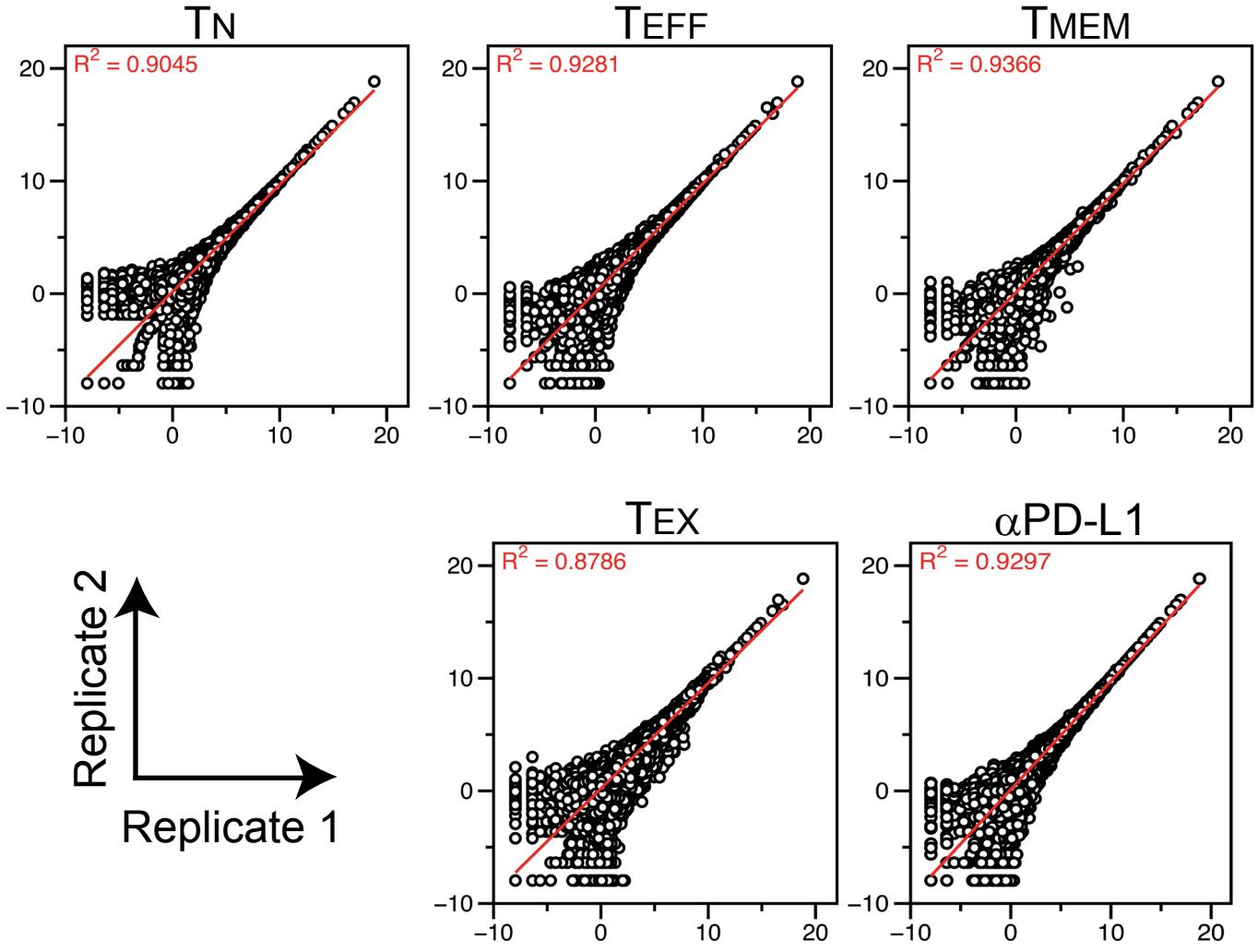

Fig. S8. Quality control analyses for ATAC-seq data. (A) Table showing total paired reads, number aligned, % aligned, and number of peaks called for each biological replicate generated for ATAC-seq. (B) Correlation of normalized ATAC-seq peak enrichment between replicate 1 and replicate 2 for each cell type. R^2 indicates the degree of correlation between replicates.

Fig. S9

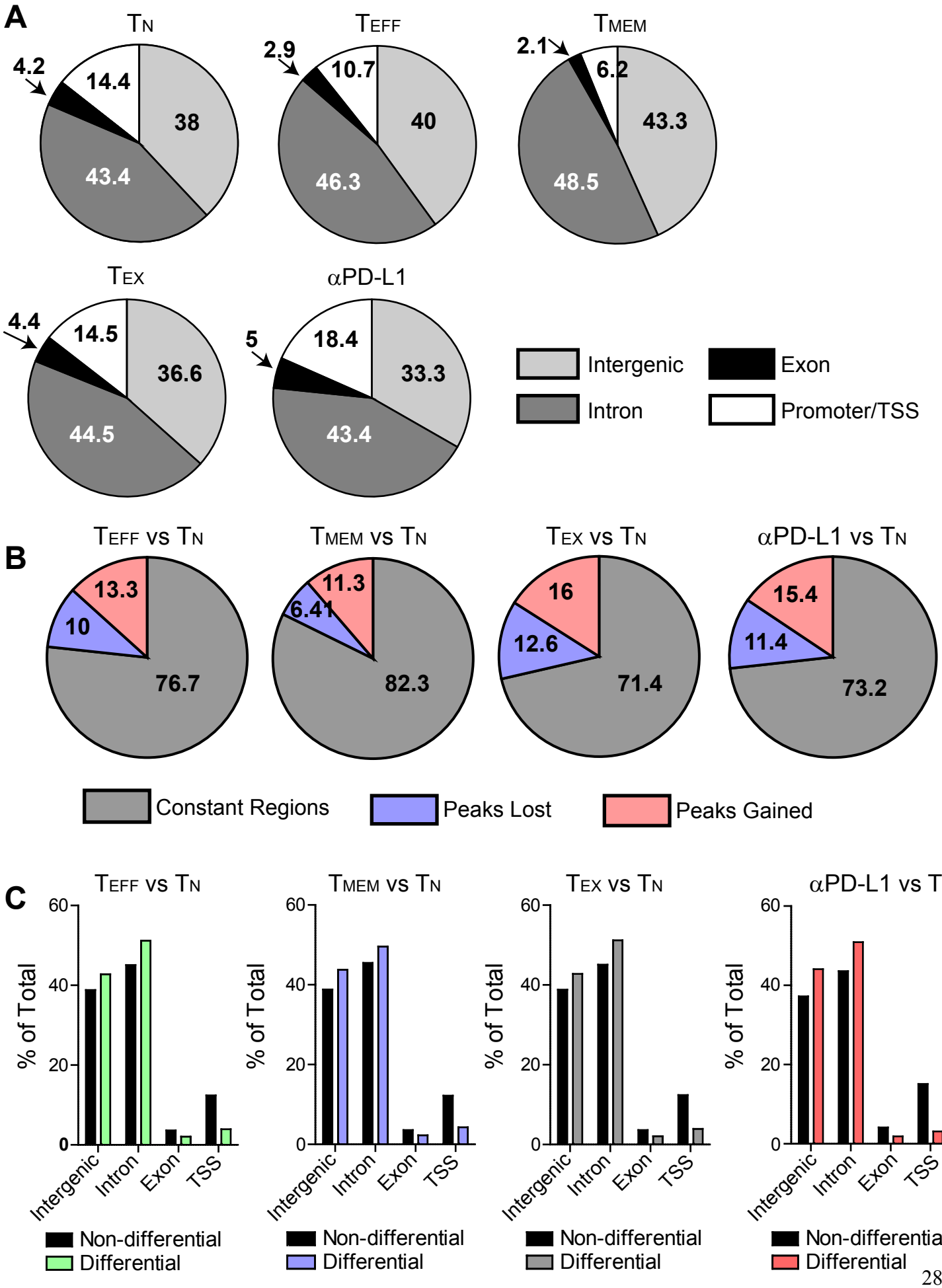
A
TN
4.2
14.4
38
43.4
TEFF
2.9
10.7
40
46.3
TMEM
2.1
6.2
43.3
48.5
TEX
4.4
14.5
36.6
44.5
αPD-L1
5
18.4
33.3
43.4
Intergenic
Exon
Intron
Promoter/TSS
B
TEFF vs TN
13.3
10
76.7
TMEM vs TN
11.3
6.41
82.3
TEX vs TN
16
12.6
71.4
αPD-L1 vs TN
15.4
11.4
73.2
Constant Regions
Peaks Lost
Peaks Gained
C
TEFF vs TN
TMEM vs TN
TEX vs TN
αPD-L1 vs TN
% of Total
60
40
20
0
Intergenic
Intron
Exon
TSS
Non-differential
Differential

Fig. S9. Region distribution of ATAC-seq data. (A) Pie charts showing the distribution of ATAC-seq peaks in intergenic, intron, exon, and promoter/TSS regions by cell type. (B) Pie charts comparing differential (LFC≥2 up (red) or down (blue)) or constant or non-differential (grey) regions of T_{EFF}, T_{MEM}, T_{EX}, or anti-PD-L1 T_{EX} relative to T_N. (C) Distribution of non-differential and differential ATAC-seq peaks compared to T_N cells (LFC≥2 up or down). Data shown are on merged replicates for each cell type.

Fig. S10

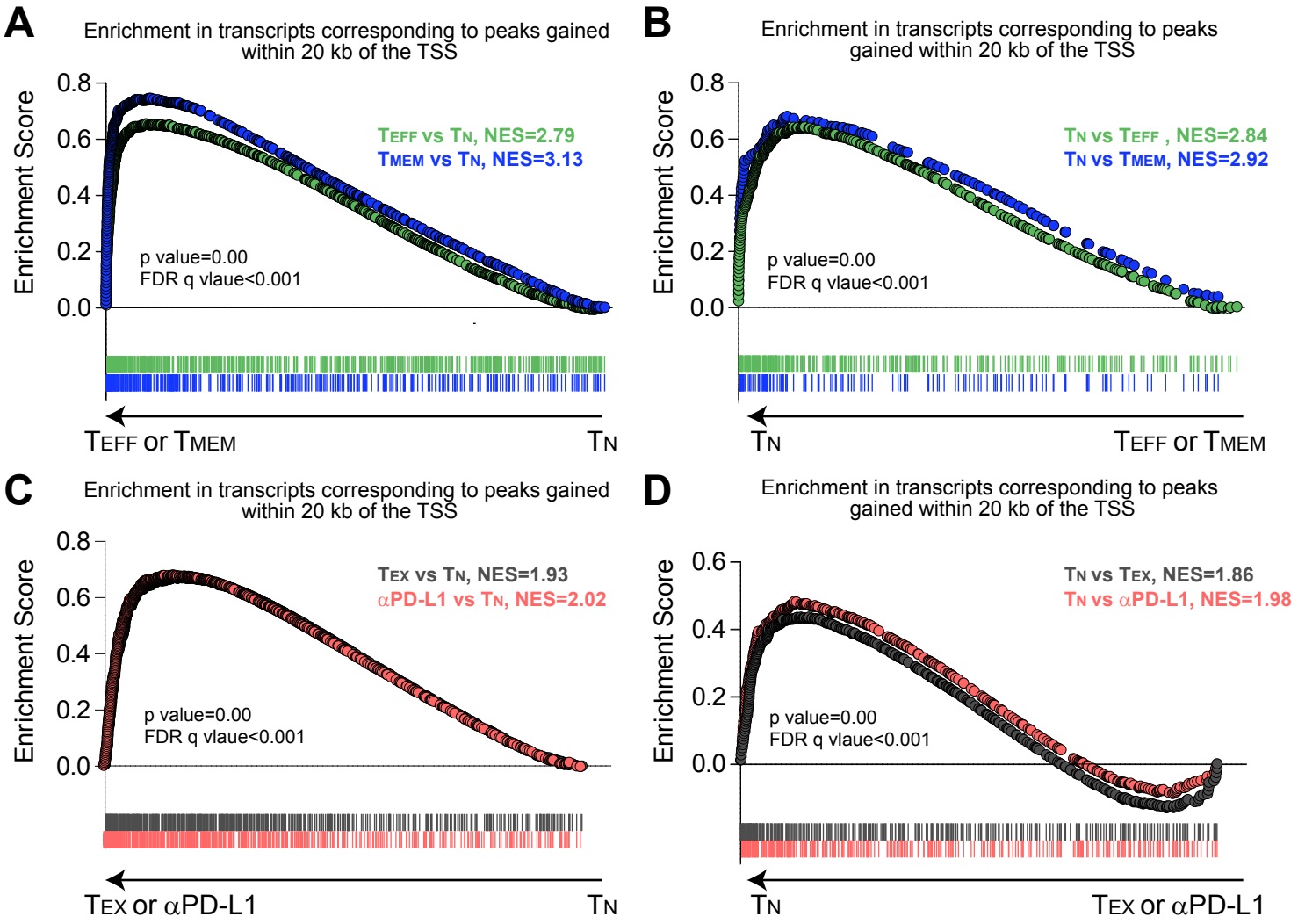
A
Enrichment in transcripts corresponding to peaks gained within 20 kb of the TSS
Enrichment Score
TEFF vs TN, NES=2.79
TMEM vs TN, NES=3.13
p value=0.00
FDR q vlaue<0.001
TEFF or TMEM
TN
B
Enrichment in transcripts corresponding to peaks gained within 20 kb of the TSS
Enrichment Score
TN vs TEFF , NES=2.84
TN vs TMEM, NES=2.92
p value=0.00
FDR q vlaue<0.001
TN
TEFF or TMEM
C
Enrichment in transcripts corresponding to peaks gained within 20 kb of the TSS
Enrichment Score
TEX vs TN, NES=1.93
αPD-L1 vs TN, NES=2.02
p value=0.00
FDR q vlaue<0.001
TEX or αPD-L1
TN
D
Enrichment in transcripts corresponding to peaks gained within 20 kb of the TSS
Enrichment Score
TN vs TEX, NES=1.86
TN vs αPD-L1, NES=1.98
p value=0.00
FDR q vlaue<0.001
TN
TEX or αPD-L1

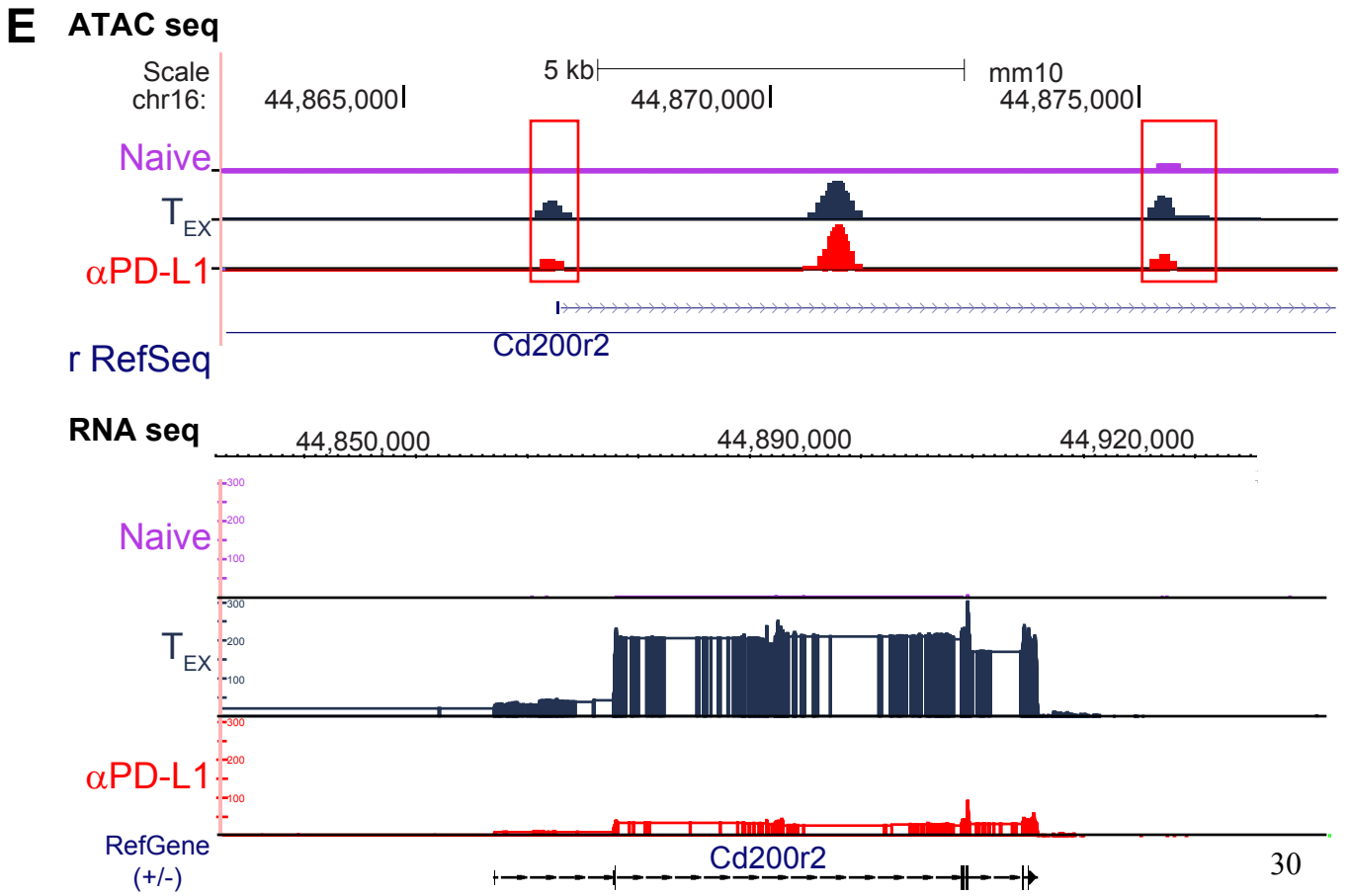
E
ATAC seq
Scale
chr16:
5 kb
mm10
44,865,000
44,870,000
44,875,000
Naive
TEX
αPD-L1
r RefSeq
Cd200r2
RNA seq
44,850,000
44,890,000
44,920,000
Naive
TEX
αPD-L1
RefGene
(+/-)
Cd200r2

Fig. S10. Increased transcription for genes near regions of open chromatin correspond in each cell type. GSEA of gene sets corresponding to OCRs identified in ATAC-seq analysis enriched in (A) T_{EFF} or T_{MEM} compared to T_N (LFC≥2) or (B) enriched in T_N compared to T_{EFF} or T_{MEM} (LFC≥2) that were within 20 kb of TSS sites. Data comparing transcription of the gene sets in (A) and (B) were obtained from (*29*). GSEA of gene sets corresponding to peaks identified in ATAC-seq analysis enriched in (C) control- or anti-PD-L1-treated T_{EX} compared to T_N (LFC≥2) or (D) enriched in T_N compared to control or anti-PD-L1-treated T_{EX} (LFC≥2) that were within 20 kb of TSS sites. The RNA-seq data was used to compare transcription of the gene sets in (C) and (D). (E) ATAC-seq and RNA-seq tracks showing the *Cd200r2* locus in T_N, control T_{EX}, and anti-PD-L1-treated T_{EX}. Tracks from one representative replicate are displayed.

Fig. S11

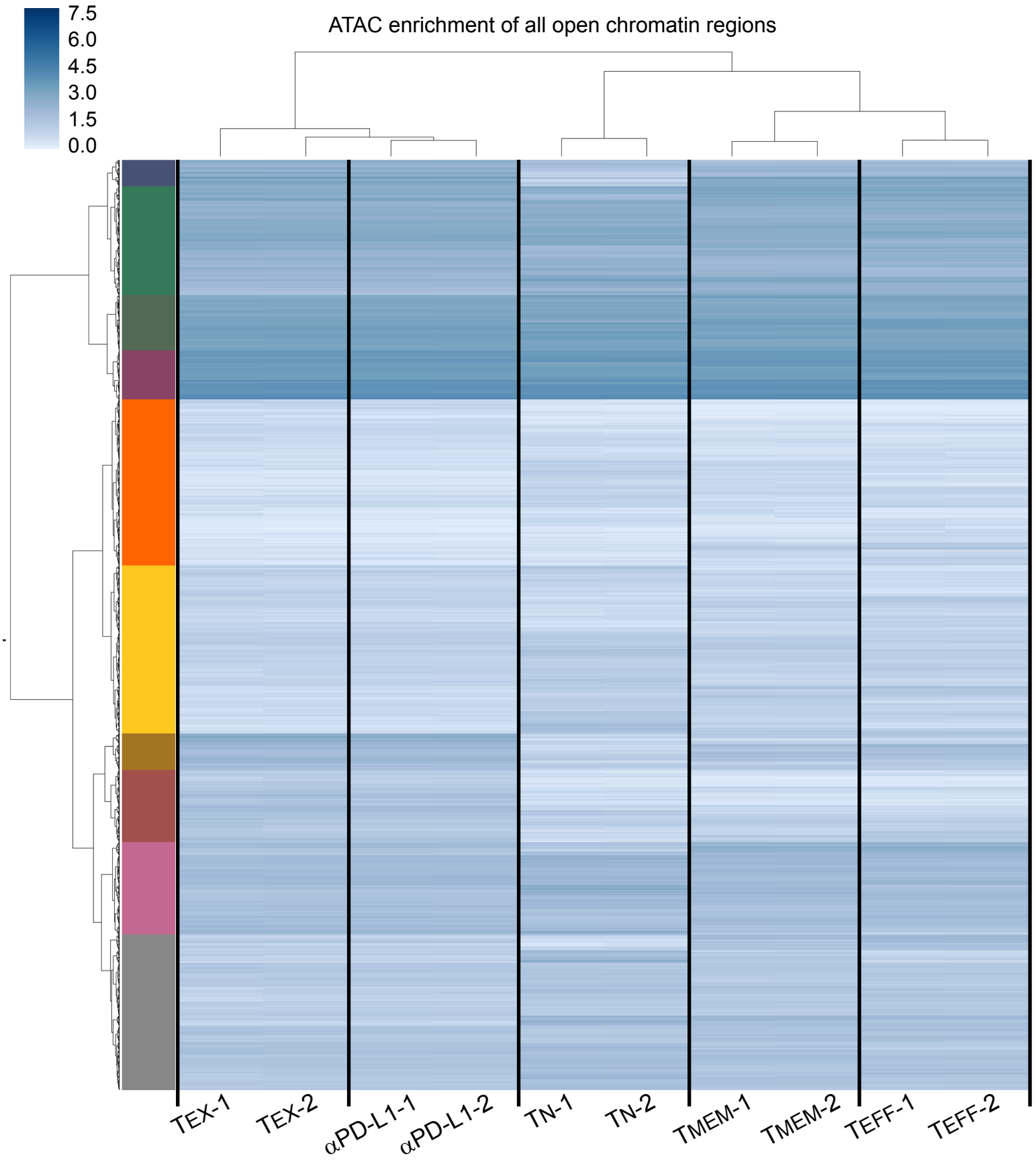
ATAC enrichment of all open chromatin regions
7.5
6.0
4.5
3.0
1.5
0.0
TEX-1
TEX-2
αPD-L1-1
αPD-L1-2
TN-1
TN-2
TMEM-1
TMEM-2
TEFF-1
TEFF-2

Fig. S11. Hierarchical clustering of all ATAC-seq open chromatin regions. Solid lines indicate separation between cell types, showing two replicates side-by-side. Row/clusters determined by flattening threshold of 90 ward clustering of Euclidean distance of input data.

Fig. S12

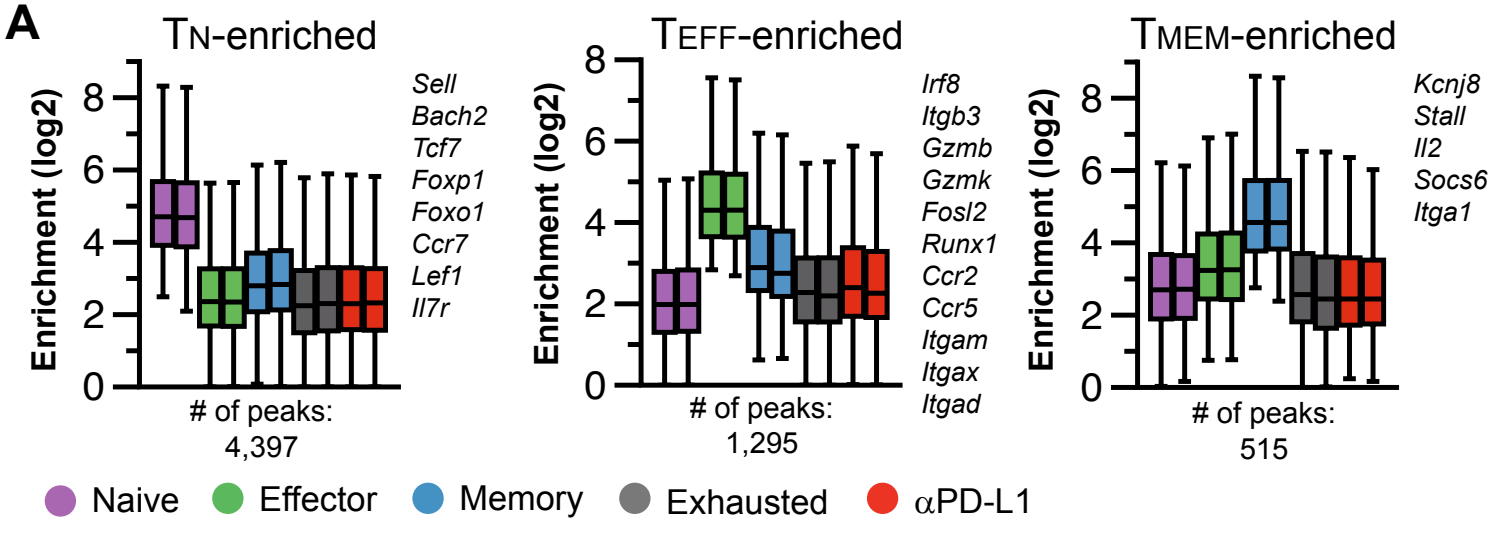
A
TN-enriched
TEFF-enriched
TMEM-enriched
Enrichment (log2)
# of peaks: 4,397
# of peaks: 1,295
# of peaks: 515
Sell
Bach2
Tcf7
Foxp1
Foxo1
Ccr7
Lef1
Il7r
Irf8
Itgb3
Gzmb
Gzmk
Fosl2
Runx1
Ccr2
Ccr5
Itgam
Itgax
Itgad
Kcnj8
Stall
Il2
Socs6
Itga1
Naive
Effector
Memory
Exhausted
αPD-L1

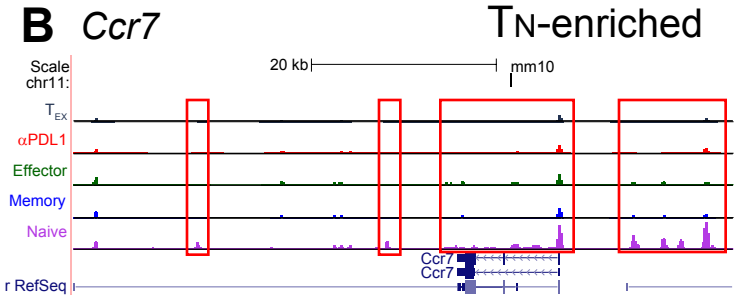
B Ccr7
TN-enriched
Scale
chr11:
20 kb
mm10
TEX
αPDL1
Effector
Memory
Naive
r RefSeq
Ccr7
Ccr7

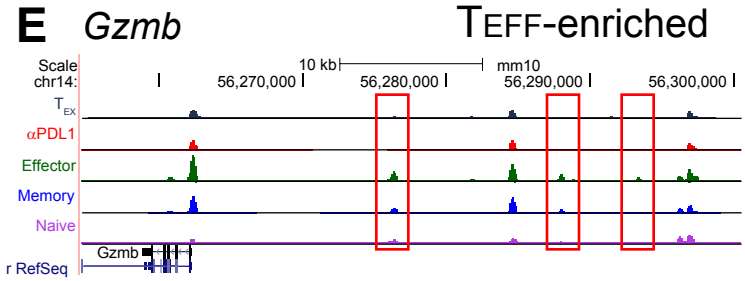
E Gzmb
TEFF-enriched
Scale
chr14:
10 kb
mm10
56,270,000
56,280,000
56,290,000
56,300,000
TEX
αPDL1
Effector
Memory
Naive
r RefSeq
Gzmb

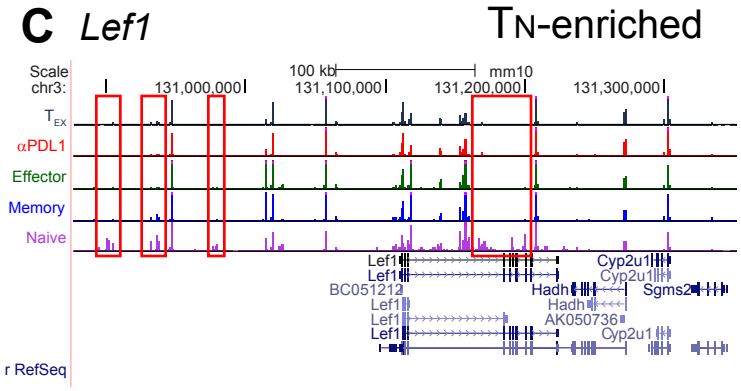
C Lef1
TN-enriched
Scale
chr3:
100 kb
mm10
131,000,000
131,100,000
131,200,000
131,300,000
TEX
αPDL1
Effector
Memory
Naive
r RefSeq
Lef1
Cyp2u1
BC051212
Hadh
Sgms2
AK050736

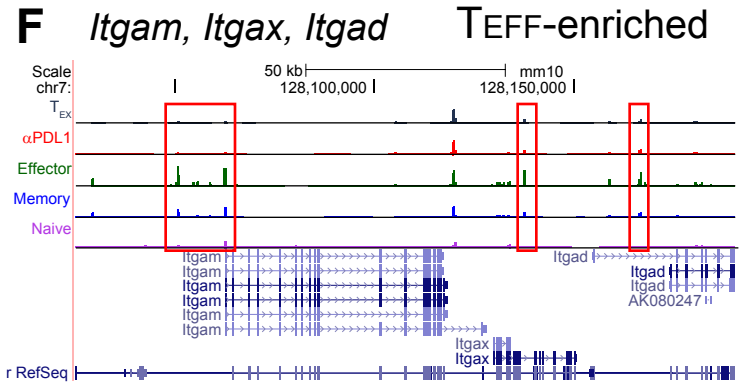
F Itgam, Itgax, Itgad
TEFF-enriched
Scale
chr7:
50 kb
mm10
128,100,000
128,150,000
TEX
αPDL1
Effector
Memory
Naive
r RefSeq
Itgam
Itgad
Itgax
AK080247

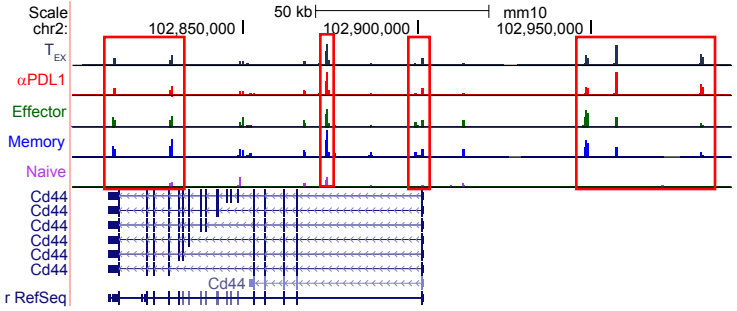
D Cd44
Activated-enriched
Scale
chr2:
50 kb
mm10
102,850,000
102,900,000
102,950,000
TEX
αPDL1
Effector
Memory
Naive
r RefSeq
Cd44

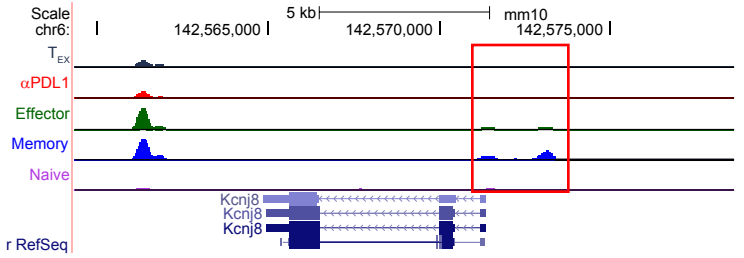
G Kcnj8
TMEM-enriched
Scale
chr6:
5 kb
mm10
142,565,000
142,570,000
142,575,000
TEX
αPDL1
Effector
Memory
Naive
r RefSeq
Kcnj8

Fig. S12. Co-cluster peak enrichment. (A) ATAC-seq enrichment of open chromatin regions (log 2) of T_N-enriched, T_{EFF}-enriched, and T_{MEM}-enriched groups from the co-cluster analysis shown in Figure 3H, corresponding with Figure 3I. Data for each replicate are shown separately. (B)-(G) Representative tracks of loci enriched in T_N, T_{EFF}, or T_{MEM}. Red boxes indicate differential peaks between the designated group and the subsequent groups. Tracks from one representative replicate are displayed.

Fig. S13

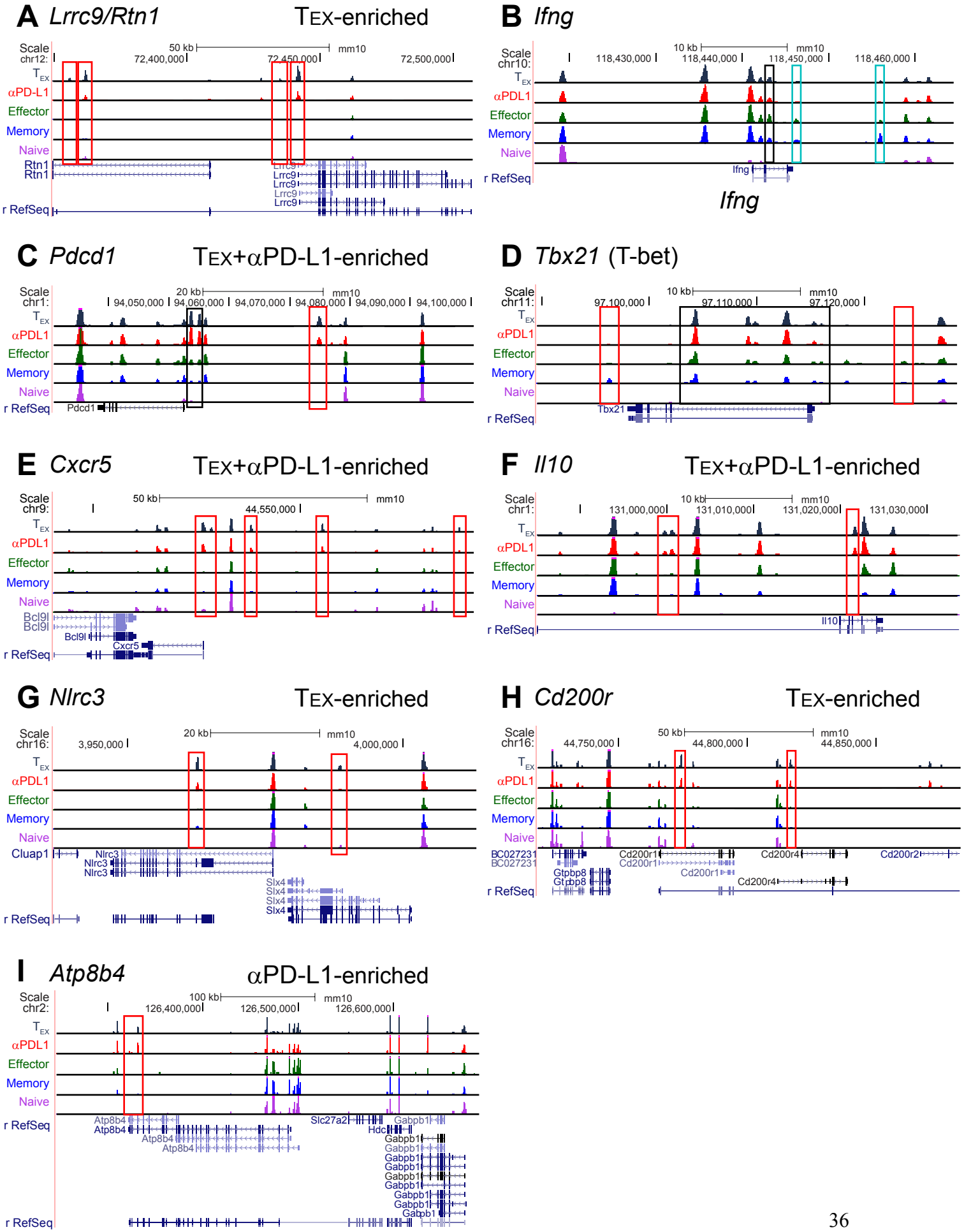
A Lrrc9/Rtn1
TEX-enriched
B Ifng
C Pdcd1
TEX+αPD-L1-enriched
D Tbx21 (T-bet)
E Cxcr5
TEX+αPD-L1-enriched
F Il10
TEX+αPD-L1-enriched
G Nlrc3
TEX-enriched
H Cd200r
TEX-enriched
I Atp8b4
αPD-L1-enriched
Scale
TEX
αPD-L1
αPDL1
Effector
Memory
Naive
r RefSeq
mm10

Fig. S13. Representative ATAC-seq Tracks. Representative tracks of different loci, enriched in control T_{EX} or anti-PD-L1-treated T_{EX} as indicated. Red boxes indicate differential peaks between the designated groups. In (B), black boxes indicate shared peaks gained in T_{EFF}, T_{MEM} and T_{EX} compared to T_N, blue boxes indicate peaks lost in T_{EX} compared to T_{EFF} and T_{MEM}. In (C), black boxes indicate peaks in the B and C regions of the *Pdcd1* locus (*22*), and red box indicates a previously unidentified OCR. (B) and (C) are shown in Figure 3G, but here also include anti-PD-L1-treated T_{EX}. Tracks from one representative replicate are displayed.

Fig. S14

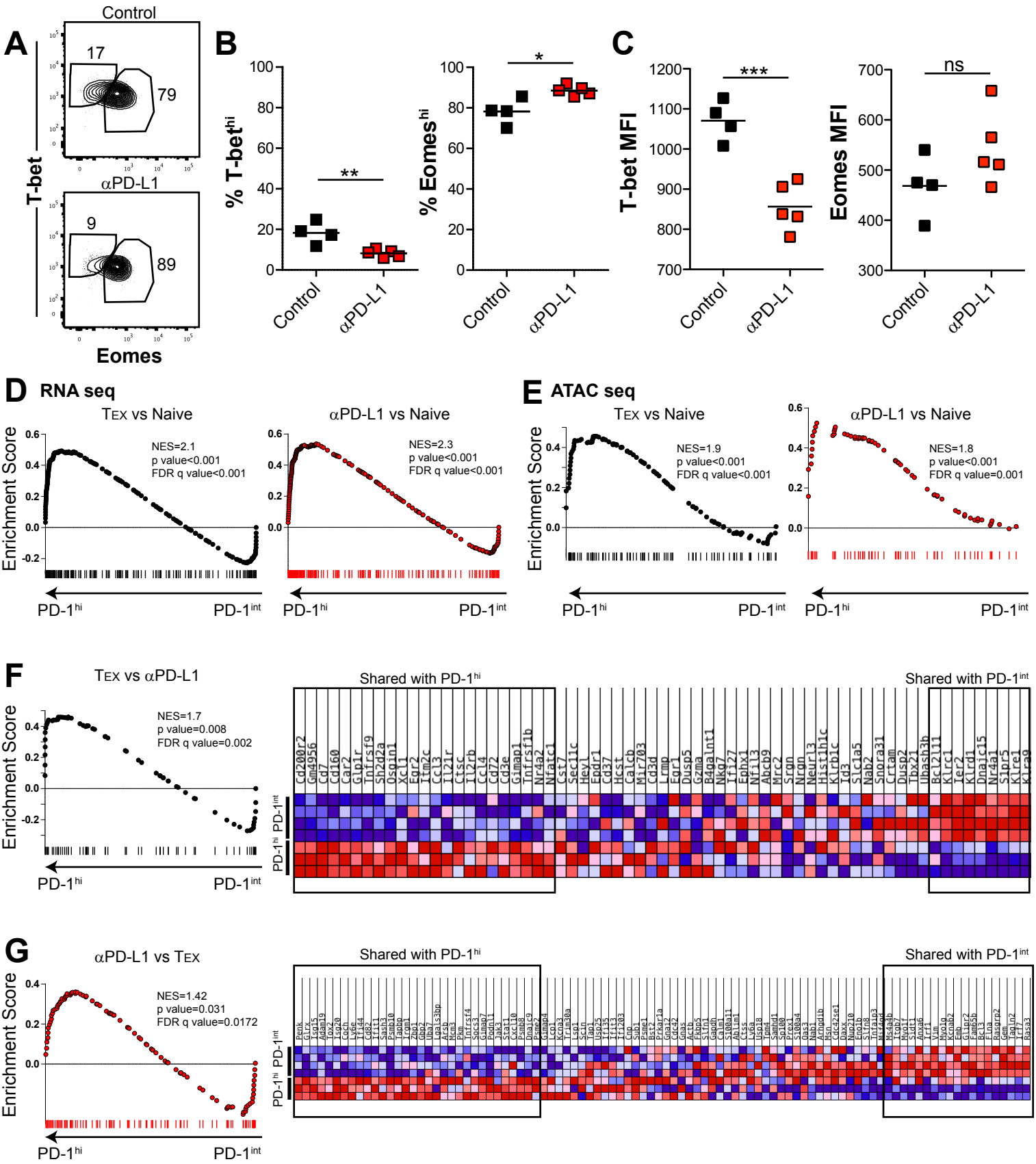
A
Control
17
79
αPD-L1
9
89
T-bet
Eomes
B
% T-bet^hi
**
% Eomes^hi
*
Control
αPD-L1
C
T-bet MFI
***
Eomes MFI
ns
D RNA seq
TEX vs Naive
NES=2.1
p value<0.001
FDR q value<0.001
αPD-L1 vs Naive
NES=2.3
p value<0.001
FDR q value<0.001
Enrichment Score
PD-1^hi
PD-1^int
E ATAC seq
TEX vs Naive
NES=1.9
p value<0.001
FDR q value<0.001
αPD-L1 vs Naive
NES=1.8
p value<0.001
FDR q value=0.001
F
TEX vs αPD-L1
NES=1.7
p value=0.008
FDR q value=0.002
Shared with PD-1^hi
Shared with PD-1^int
G
αPD-L1 vs TEX
NES=1.42
p value=0.031
FDR q value=0.0172
Shared with PD-1^hi
Shared with PD-1^int

Fig. S14. Epigenetic and transcriptional profiles for control- and anti-PD-L1 treated T_{EX} are enriched for features of the Eomes^{hi} PD-1^{hi} T_{EX} subset. (A) Representative flow cytometry plots gated on P14 cells showing T-bet and Eomes expression. Numbers indicate frequency of each population of the parent P14 population. (B) Quantification of the frequency of T-bet^{hi} and Eomes^{hi} subsets shown in (A) following anti-PD-L1 treatment. (C) Quantification of the geometric MFI of T-bet and Eomes in the mice shown in (B). Data are representative of three independent experiments with at least four mice per group. Asterisks indicating significance determined by unpaired t tests between groups are *$p<0.05$, **$p<0.01$, and ***$p<0.001$. (D) GSEA comparing the genes enriched in T_{EX} compared to T_N or anti-PD-L1 versus T_N (LFC$\geq$2, $p<0.05$, top 200) to the transcriptional profiles of PD-1^{int} (T-bet^{hi}) or PD-1^{hi} (Eomes^{hi}) cells. (E) GSEA comparing the genes near open chromatin regions enriched in T_{EX} compared to T_N or anti-PD-L1 versus T_N (LFC$\geq$4, $p<0.05$) to the transcriptional profiles of PD-1^{int} or PD-1^{hi} cells. GSEA (left) comparing the genes enriched in (F) T_{EX} compared to anti-PD-L1 or (G) anti-PD-L1 compared to T_{EX} (LFC$\geq$2, $p<0.05$) to the transcriptional profiles of PD-1^{int} (T-bet^{hi}) or PD-1^{hi} (Eomes^{hi}) cells. Heat maps of individual genes shown to the right. Transcriptional profiles for PD-1^{int} and PD-1^{hi} cells obtained from (*29*).

Fig. S15

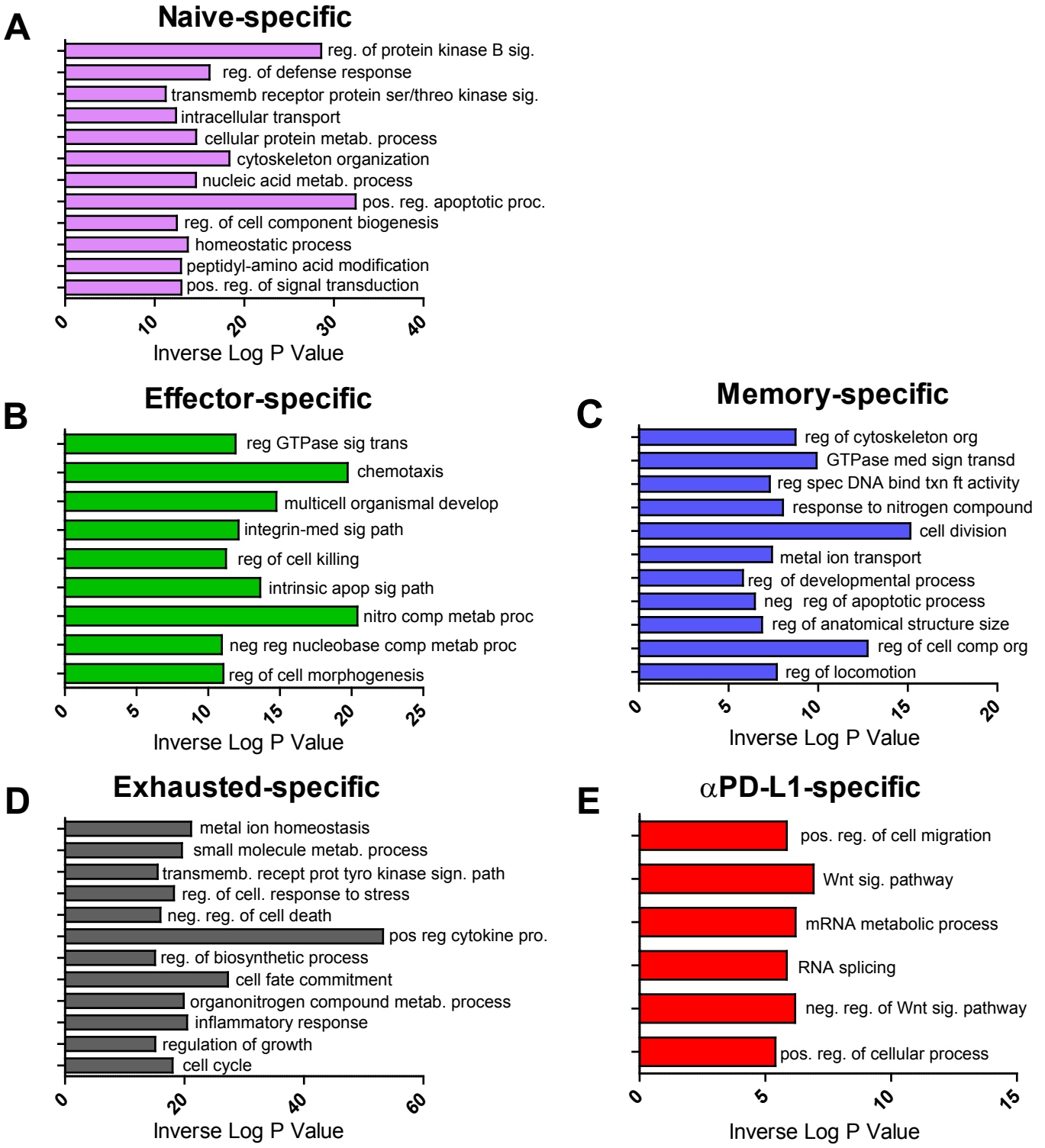
A
Naive-specific
reg. of protein kinase B sig.
reg. of defense response
transmemb receptor protein ser/threo kinase sig.
intracellular transport
cellular protein metab. process
cytoskeleton organization
nucleic acid metab. process
pos. reg. apoptotic proc.
reg. of cell component biogenesis
homeostatic process
peptidyl-amino acid modification
pos. reg. of signal transduction
0 10 20 30 40
Inverse Log P Value
B
Effector-specific
reg GTPase sig trans
chemotaxis
multicell organismal develop
integrin-med sig path
reg of cell killing
intrinsic apop sig path
nitro comp metab proc
neg reg nucleobase comp metab proc
reg of cell morphogenesis
0 5 10 15 20 25
Inverse Log P Value
C
Memory-specific
reg of cytoskeleton org
GTPase med sign transd
reg spec DNA bind txn ft activity
response to nitrogen compound
cell division
metal ion transport
reg of developmental process
neg reg of apoptotic process
reg of anatomical structure size
reg of cell comp org
reg of locomotion
0 5 10 15 20
Inverse Log P Value
D
Exhausted-specific
metal ion homeostasis
small molecule metab. process
transmemb. recept prot tyro kinase sign. path
reg. of cell. response to stress
neg. reg. of cell death
pos reg cytokine pro.
reg. of biosynthetic process
cell fate commitment
organonitrogen compound metab. process
inflammatory response
regulation of growth
cell cycle
0 20 40 60
Inverse Log P Value
E
αPD-L1-specific
pos. reg. of cell migration
Wnt sig. pathway
mRNA metabolic process
RNA splicing
neg. reg. of Wnt sig. pathway
pos. reg. of cellular process
0 5 10 15
Inverse Log P Value

Fig. S15. Co-cluster GO terms. (A)-(E) Selected significantly enriched ($p<0.05$) GO terms associated with peaks from each cell type. Shown are terms that were associated with only one cell type identified using REVIGO (see Materials and Methods). A complete list of GO terms for each cell type can be found in Table S8. GO terms were identified on merged replicates.

Fig. S16

TFs in TEX Network

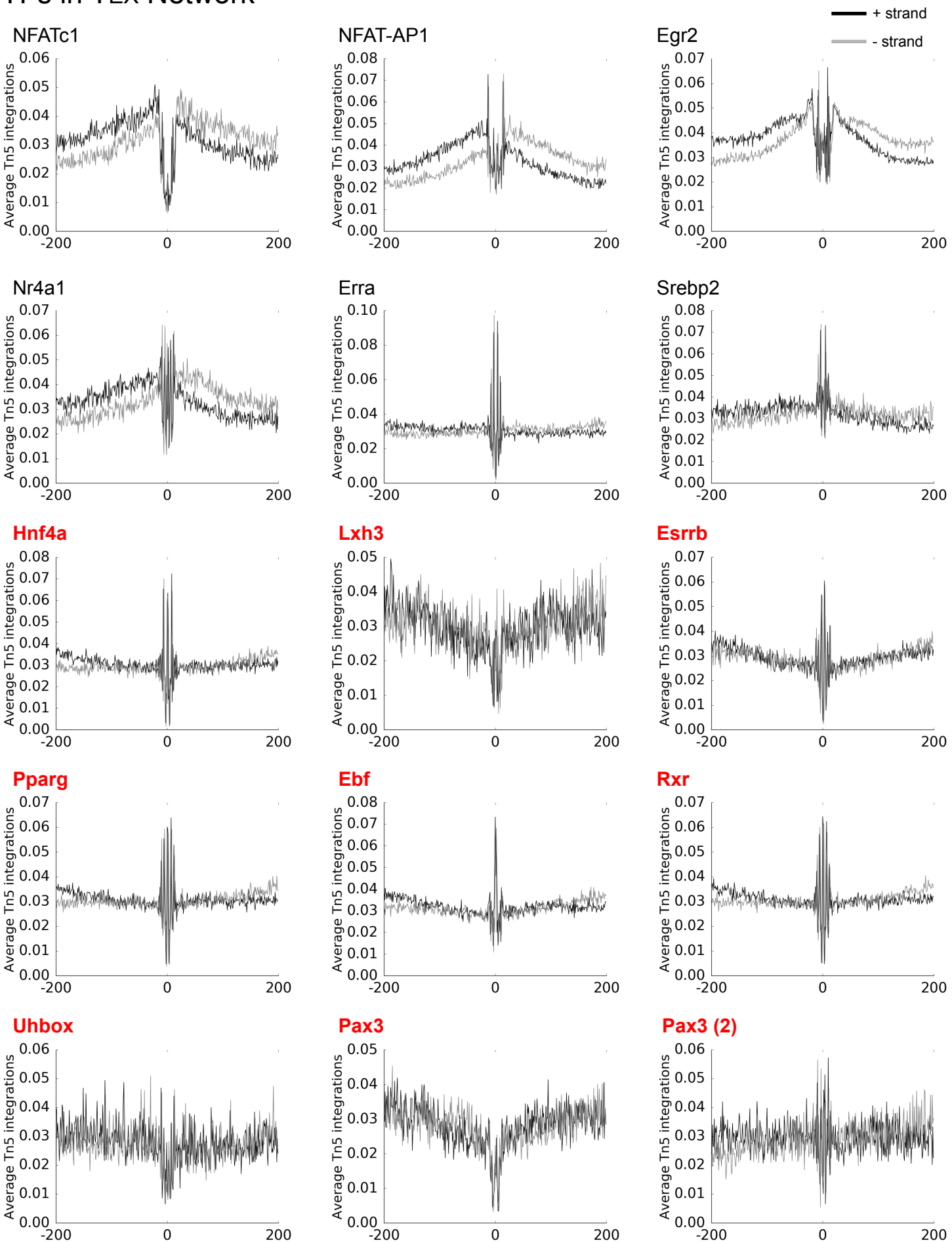

Fig. S16. Transcription factor footprinting in control-treated T_{EX} cells. Transcription factor footprinting was performed on merged replicates (see Materials and Methods) for the indicated transcription factors using the ATAC-seq data from control treated T_{EX}. Transcription factors shown were identified using Wellington bootstrap analysis in Figure 4B. Red lettering indicates transcription factors that were excluded from downstream network analysis due to lack of evidence of binding in the footprinting analysis and based on selection criteria described in Materials and Methods.

Fig. S17

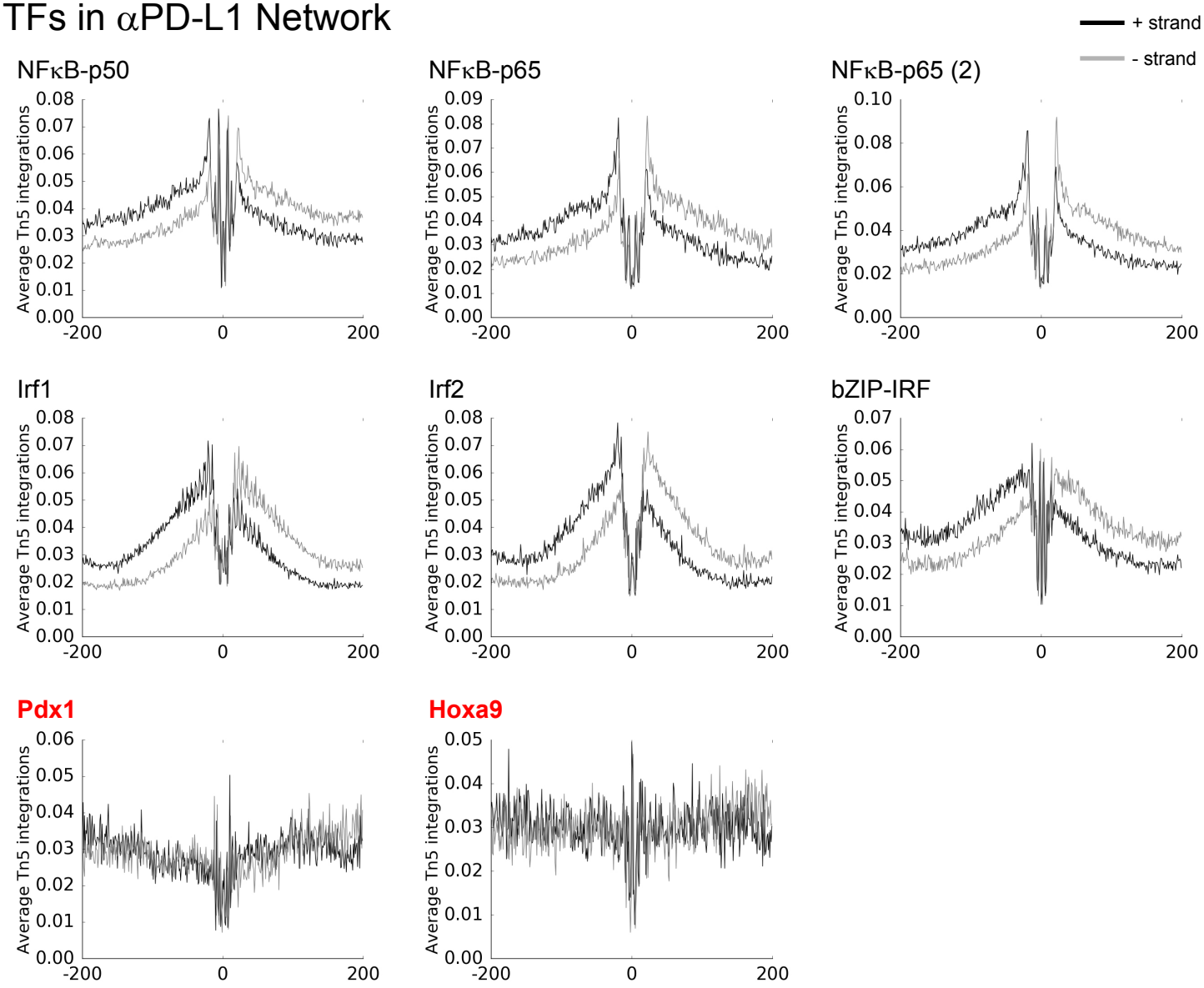
TFs in αPD-L1 Network
+ strand
- strand
NFκB-p50
NFκB-p65
NFκB-p65 (2)
Irf1
Irf2
bZIP-IRF
Pdx1
Hoxa9
Average Tn5 integrations
-200
0
200

Fig. S17. Transcription factor footprinting in anti-PD-L1-treated T_{EX} cells.

Transcription factor footprinting was performed on merged replicates (see Materials and Methods) for the indicated transcription factors using the ATAC-seq data from anti-PD-L1 treated T_{EX}. Transcription factors shown were identified using Wellington bootstrap analysis in Figure 4B. Red lettering indicates transcription factors that were excluded from downstream network analysis due to lack of evidence of binding in the footprinting analysis and based on selection criteria described in Materials and Methods.

Fig. S18

A TFs predicted to bind promoter regions of top differentially expressed genes UP with anti-PD-L1

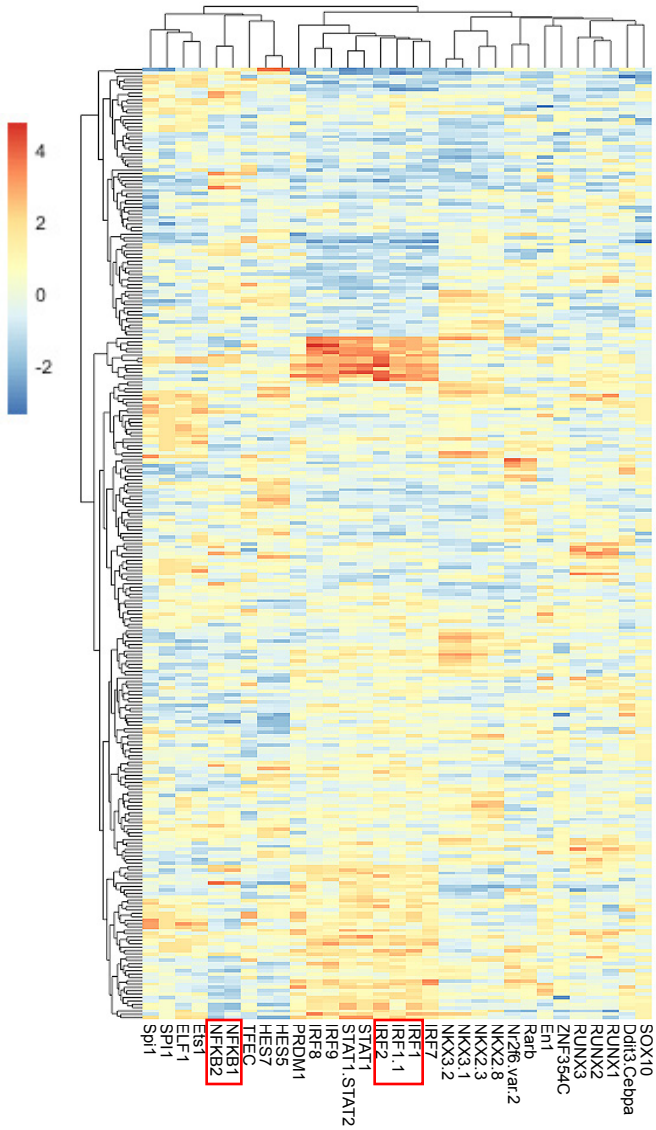

Shared with αPD-L1 UP Network:
NFκB, IRF1, IRF2

B TFs predicted to bind promoter regions of top differentially expressed genes DOWN with anti-PD-L1

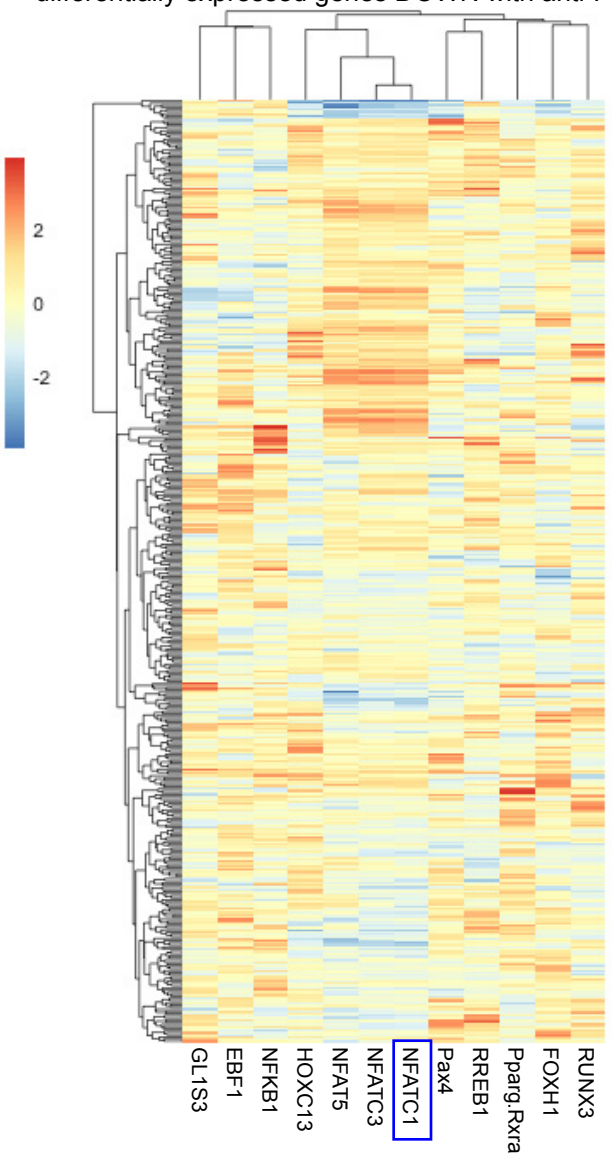

Shared with αPD-L1 DOWN Network:
NFATc1

Fig. S18. Predicted transcription factors involved in regulating differentially expressed genes in re-invigorated T_{EX} following anti-PD-L1 treatment. The differentially expressed genes up (A) or down (B) by microarray after 2 weeks of anti-PD-L1 treatment ($p<0.05$, LFC$\geq$0.3) (y-axis) and the transcription factors predicted to bind the promoter regions of these genes (x-axis) identified using PSCAN analysis. Transcription factors identified using this analysis that are shared with the transcription factors identified in Figure 4B-D are listed underneath each heat map. Complete list of genes corresponding to different transcription factors is available in Table S12.

Excel Table Legends

Table S1. List of genes significantly differentially expressed following anti-PD-L1 treatment. This table is associated with Figure S1D, showing entire list of genes statistically significantly differentially expressed ($p<0.05$) one day following the two week treatment period with anti-PD-L1 treatment in the microarray. Expression is shown as $\log_2$ fold change of anti-PD-L1 T_{EX}/control T_{EX}. Positive log fold change values indicate increased expression following anti-PD-L1, negative values indicate decreased expression.

Table S2: GSEA reports showing GO and KEGG pathways identified following anti-PD-L1 treatment. GSEA reports from the microarray analysis comparing anti-PD-L1 and control T_{EX} one day after cessation of treatment. This table is associated with Figure 1B. There are four tabs, two of GSEA reports for control T_{EX} and two of GSEA reports for anti-PD-L1-treated T_{EX}, one each for GO terms and one for KEGG pathways.

Table S3: Gene list and GSEA report for effector genes. This table is associated with Figure 1C. There are two tabs. The first is the gene list of "effector" genes, identified as up in CD8 T cells at day 6 post-LCMV Arm compared to naïve T cells, with genes associated with six of the major GO terms corresponding to cell cycle (cell cycle, mitosis, spindle, DNA replication, mitotic cell cycle, and cell cycle) removed. The second tab is the GSEA report for anti-PD-L1 compared to control T_{EX} from the microarray using the gene list in the first tab.

Table S4: List of genes identified using Leading Edge Metagene analysis and overlaps between cell types. This table is associated with Figure 1E and Figure S1E and S1F. There are three tabs. One contains lists of genes associated with the metagenes identified for each comparison (anti-PD-L1 versus T_{EX}, T_{EFF} versus T_N, T_{MEM} versus T_N, and T_{EX} versus T_N). Another contains the GO annotations corresponding to the genes in each metagene. The third details the overlaps between metagenes identified for different cell types as a matrix, with the metagenes for anti-PD-L1 versus T_{EX} on the vertical axis, and T_{EFF} versus T_N, T_{MEM} versus T_N, and T_{EX} versus T_N on the horizontal axis.

Table S5: Differentially expressed genes one day or 18-29 weeks after cessation of anti-PD-L1 treatment in the RNA-seq data set. This table is associated with Figure S6. There are 5 tabs. The first represents Figure S6B, showing the 50 unique neighbors by class comparison for control or anti-PD-L1 treated cells one day or 18-29 weeks after treatment. The remaining tabs represent Figure S6C, showing pairwise comparisons of significant genes ($p<0.05$) that are differentially expressed ($LFC \leq 0.58$) between each pair. Comparisons include day $^+1$ control versus anti-PD-L1, control day $^+1$ versus 18-29 weeks, anti-PD-L1 day $^+1$ versus 18-29 weeks, 18-29 weeks control versus anti-PD-L1.

Table S6: GO term enrichments in the RNA-seq data set. GSEA report for GO terms enriched in RNA seq data set. This table is associated with Figures S5E and S6E. There are 9 tabs. The first tab is a legend describing the pairwise comparisons shown in each report. Comparisons include day $^+1$ control versus anti-PD-L1, control day $^+1$ versus 18-

29 weeks, anti-PD-L1 day $^{+}$1 versus 18-29 weeks, 18-29 weeks control versus anti-PD-L1.

Table S7: List of ATAC-seq peaks annotated with nearest genes corresponding to distinct co-clusters. This table is associated with Figure 3H and 3I and Figure S12A. There are seven tabs, corresponding to the seven co-clusters (enriched in T_N, T_{EFF}, T_{MEM}, both T_{EFF} and T_{MEM} shared, T_{EX}, anti-PD-L1-treated T_{EX}, and both T_{EX} and anti-PD-L1-treated T_{EX} shared). Nearest gene and distance to TSS are indicated.

Table S8: GO terms associated with ATAC-seq peaks gained exclusive to each cell type. This table is associated with Figure S15. Statistically significant GO term enrichment corresponding to the genes associated with peaks found in each cell type were identified as described in the Materials and Methods. The GO terms highlighted in yellow are also listed in Figure S15, and were selected based on significant p values and elevated number of genes in each pathway.

Table S9: Full list of transcription factor binding motifs present in open chromatin regions gained or lost in T_{EX} following anti-PD-L1 treatment. This table is associated with Figure 4A, and contains the full list of transcription factor binding motifs, the corresponding consensus sequence, the percentage of peaks changed containing the motif, and the percentage of background peaks containing the motif. There are two tabs, one each containing motifs in peaks gained and lost in T_{EX} following anti-PD-L1 treatment.

Table S10: Full list of transcription factors predicted to have uniquely enriched binding in OCRs in T_N, T_{EFF}, T_{MEM}, T_{EX}, or anti-PD-L1-treated T_{EX}. Summary of Wellington bootstrap analysis displayed as a heat map in Figure 4B. Top 10 enriched TFs for each cell type are listed.

Table S11: Association of differentially expressed genes with transcription factors predicted to have altered activity in ATAC-seq data set. This table is associated with the integrated epigenetic/transcriptional network shown in Figure 4D. This table lists the TFs predicted to have increased or decreased activity following anti-PD-L1 treatment determined used the ATAC-seq data, and the corresponding genes predicted to be regulated by those TFs that were differentially expressed following anti-PD-L1 treatment (LFC$\geq$0.3 up or down) in the microarray. For LFC, positive values indicate increased expression with anti-PD-L1, decreased values indicate decreased expression with anti-PD-L1.

Table S12: Transcription factors predicted to regulate differentially expressed genes following anti-PD-L1. This table is associated with Figure S18. It has 4 tabs. These data were generated independently of the ATAC-seq data set and were used as a validation of the integrated epigenetic/transcriptional network (Figure 4D). We started with the list of differentially expressed genes up or down following anti-PD-L1 in the microarray (two of four tabs). We then used PSCAN to identify TFs in the promoter regions of these genes predicted to bind (other two of four tabs).

References and Notes

1. E. J. Wherry, M. Kurachi, Molecular and cellular insights into T cell exhaustion. *Nat. Rev. Immunol.* **15**, 486–499 (2015). doi:10.1038/nri3862 Medline

2. D. B. Page, M. A. Postow, M. K. Callahan, J. P. Allison, J. D. Wolchok, Immune modulation in cancer with antibodies. *Annu. Rev. Med.* **65**, 185–202 (2014). doi:10.1146/annurev-med-092012-112807 Medline

3. P. Sharma, J. P. Allison, The future of immune checkpoint therapy. *Science* **348**, 56–61 (2015). doi:10.1126/science.aaa8172 Medline

4. D. S. Shin, A. Ribas, The evolution of checkpoint blockade as a cancer therapy: What's here, what's next? *Curr. Opin. Immunol.* **33**, 23–35 (2015). doi:10.1016/j.coi.2015.01.006 Medline

5. D. L. Barber, E. J. Wherry, D. Masopust, B. Zhu, J. P. Allison, A. H. Sharpe, G. J. Freeman, R. Ahmed, Restoring function in exhausted CD8 T cells during chronic viral infection. *Nature* **439**, 682–687 (2006). doi:10.1038/nature04444 Medline

6. See supplementary information on *Science* Online.

7. M. M. Gubin, X. Zhang, H. Schuster, E. Caron, J. P. Ward, T. Noguchi, Y. Ivanova, J. Hundal, C. D. Arthur, W.-J. Krebber, G. E. Mulder, M. Toebes, M. D. Vesely, S. S. K. Lam, A. J. Korman, J. P. Allison, G. J. Freeman, A. H. Sharpe, E. L. Pearce, T. N. Schumacher, R. Aebersold, H.-G. Rammensee, C. J. M. Melief, E. R. Mardis, W. E. Gillanders, M. N. Artyomov, R. D. Schreiber, Checkpoint blockade cancer immunotherapy targets tumour-specific mutant antigens. *Nature* **515**, 577–581 (2014). doi:10.1038/nature13988 Medline

8. B. Bengsch, A. L. Johnson, M. Kurachi, P. M. Odorizzi, K. E. Pauken, J. Attanasio, E. Stelekati, L. M. McLane, M. A. Paley, G. M. Delgoffe, E. J. Wherry, Bioenergetic insufficiencies due to metabolic alterations regulated by the inhibitory receptor PD-1 are an early driver of $CD8^+$ T cell exhaustion. *Immunity* **45**, 358–373 (2016). doi:10.1016/j.immuni.2016.07.008 Medline

9. M. M. Staron, S. M. Gray, H. D. Marshall, I. A. Parish, J. H. Chen, C. J. Perry, G. Cui, M. O. Li, S. M. Kaech, The transcription factor FoxO1 sustains expression of the inhibitory receptor PD-1 and survival of antiviral $CD8^+$ T cells during chronic infection. *Immunity* **41**, 802–814 (2014). doi:10.1016/j.immuni.2014.10.013 Medline

10. N. Patsoukis, J. Brown, V. Petkova, F. Liu, L. Li, V. A. Boussiotis, Selective effects of PD-1 on Akt and Ras pathways regulate molecular components of the cell cycle and inhibit T cell proliferation. *Sci. Signal.* **5**, ra46 (2012). doi:10.1126/scisignal.2002796 Medline

11. J. Godec, Y. Tan, A. Liberzon, P. Tamayo, S. Bhattacharya, A. J. Butte, J. P. Mesirov, W. N. Haining, Compendium of immune signatures identifies conserved and species-specific biology in response to inflammation. *Immunity* **44**, 194–206 (2016). doi:10.1016/j.immuni.2015.12.006 Medline

12. H. Shin, S. D. Blackburn, J. N. Blattman, E. J. Wherry, Viral antigen and extensive division maintain virus-specific CD8 T cells during chronic infection. *J. Exp. Med.* **204**, 941–949 (2007). doi:10.1084/jem.20061937 Medline

13. E. J. Wherry, D. L. Barber, S. M. Kaech, J. N. Blattman, R. Ahmed, Antigen-independent memory CD8 T cells do not develop during chronic viral infection. *Proc. Natl. Acad. Sci. U.S.A.* **101**, 16004–16009 (2004). doi:10.1073/pnas.0407192101 Medline

14. M. Pellegrini, T. Calzascia, J. G. Toe, S. P. Preston, A. E. Lin, A. R. Elford, A. Shahinian, P. A. Lang, K. S. Lang, M. Morre, B. Assouline, K. Lahl, T. Sparwasser, T. F. Tedder, J. H. Paik, R. A. DePinho, S. Basta, P. S. Ohashi, T. W. Mak, IL-7 engages multiple mechanisms to overcome chronic viral infection and limit organ pathology. *Cell* **144**, 601–613 (2011). doi:10.1016/j.cell.2011.01.011 Medline

15. S. G. Nanjappa, E. H. Kim, M. Suresh, Immunotherapeutic effects of IL-7 during a chronic viral infection in mice. *Blood* **117**, 5123–5132 (2011). doi:10.1182/blood-2010-12-323154 Medline

16. B. Youngblood, K. J. Oestreich, S.-J. Ha, J. Duraiswamy, R. S. Akondy, E. E. West, Z. Wei, P. Lu, J. W. Austin, J. L. Riley, J. M. Boss, R. Ahmed, Chronic virus infection enforces demethylation of the locus that encodes PD-1 in antigen-specific $CD8^+$ T cells. *Immunity* **35**, 400–412 (2011). doi:10.1016/j.immuni.2011.06.015 Medline

17. D. T. Utzschneider, A. Legat, S. A. Fuertes Marraco, L. Carrié, I. Luescher, D. E. Speiser, D. Zehn, T cells maintain an exhausted phenotype after antigen withdrawal and population reexpansion. *Nat. Immunol.* **14**, 603–610 (2013). doi:10.1038/ni.2606 Medline

18. J. M. Angelosanto, S. D. Blackburn, A. Crawford, E. J. Wherry, Progressive loss of memory T cell potential and commitment to exhaustion during chronic viral infection. *J. Virol.* **86**, 8161–8170 (2012). doi:10.1128/JVI.00889-12 Medline

19. F. Zhang, X. Zhou, J. R. DiSpirito, C. Wang, Y. Wang, H. Shen, Epigenetic manipulation restores functions of defective $CD8^+$ T cells from chronic viral infection. *Mol. Ther.* **22**, 1698–1706 (2014). doi:10.1038/mt.2014.91 Medline

20. J. D. Buenrostro, P. G. Giresi, L. C. Zaba, H. Y. Chang, W. J. Greenleaf, Transposition of native chromatin for fast and sensitive epigenomic profiling of open chromatin, DNA-binding proteins and nucleosome position. *Nat. Methods* **10**, 1213–1218 (2013). doi:10.1038/nmeth.2688 Medline

21. D. R. Winter, I. Amit, The role of chromatin dynamics in immune cell development. *Immunol. Rev.* **261**, 9–22 (2014). doi:10.1111/imr.12200 Medline

22. K. J. Oestreich, H. Yoon, R. Ahmed, J. M. Boss, NFATc1 regulates PD-1 expression upon T cell activation. *J. Immunol.* **181**, 4832–4839 (2008). doi:10.4049/jimmunol.181.7.4832 Medline

23. C. Kao, K. J. Oestreich, M. A. Paley, A. Crawford, J. M. Angelosanto, M.-A. A. Ali, A. M. Intlekofer, J. M. Boss, S. L. Reiner, A. S. Weinmann, E. J. Wherry, Transcription factor T-bet represses expression of the inhibitory receptor PD-1 and sustains virus-specific CD8+ T cell responses during chronic infection. *Nat. Immunol.* **12**, 663–671 (2011). doi:10.1038/ni.2046 Medline

24. M. A. Paley, D. C. Kroy, P. M. Odorizzi, J. B. Johnnidis, D. V. Dolfi, B. E. Barnett, E. K. Bikoff, E. J. Robertson, G. M. Lauer, S. L. Reiner, E. J. Wherry, Progenitor and terminal subsets of CD8+ T cells cooperate to contain chronic viral infection. *Science* **338**, 1220–1225 (2012). doi:10.1126/science.1229620 Medline

25. S. D. Blackburn, H. Shin, G. J. Freeman, E. J. Wherry, Selective expansion of a subset of exhausted CD8 T cells by αPD-L1 blockade. *Proc. Natl. Acad. Sci. U.S.A.* **105**, 15016–15021 (2008). doi:10.1073/pnas.0801497105 Medline

26. R. He, S. Hou, C. Liu, A. Zhang, Q. Bai, M. Han, Y. Yang, G. Wei, T. Shen, X. Yang, L. Xu, X. Chen, Y. Hao, P. Wang, C. Zhu, J. Ou, H. Liang, T. Ni, X. Zhang, X. Zhou, K. Deng, Y. Chen, Y. Luo, J. Xu, H. Qi, Y. Wu, L. Ye, Follicular CXCR5-expressing $CD8^+$ T cells curtail chronic viral infection. *Nature* **537**, 412–428 (2016). doi:10.1038/nature19317 Medline

27. S. J. Im, M. Hashimoto, M. Y. Gerner, J. Lee, H. T. Kissick, M. C. Burger, Q. Shan, J. S. Hale, J. Lee, T. H. Nasti, A. H. Sharpe, G. J. Freeman, R. N. Germain, H. I. Nakaya, H.-H. Xue, R. Ahmed, Defining $CD8^+$ T cells that provide the proliferative burst after PD-1 therapy. *Nature* **537**, 417–421 (2016). doi:10.1038/nature19330 Medline

28. D. T. Utzschneider, M. Charmoy, V. Chennupati, L. Pousse, D. P. Ferreira, S. Calderon-Copete, M. Danilo, F. Alfei, M. Hofmann, D. Wieland, S. Pradervand, R. Thimme, D. Zehn, W. Held, T cell factor 1-expressing memory-like $CD8^+$ T cells sustain the immune response to chronic viral infections. *Immunity* **45**, 415–427 (2016). doi:10.1016/j.immuni.2016.07.021 Medline

29. T. A. Doering, A. Crawford, J. M. Angelosanto, M. A. Paley, C. G. Ziegler, E. J. Wherry, Network analysis reveals centrally connected genes and pathways involved in CD8+ T cell exhaustion versus memory. *Immunity* **37**, 1130–1144 (2012). doi:10.1016/j.immuni.2012.08.021 Medline

30. G. J. Martinez, R. M. Pereira, T. Äijö, E. Y. Kim, F. Marangoni, M. E. Pipkin, S. Togher, V. Heissmeyer, Y. C. Zhang, S. Crotty, E. D. Lamperti, K. M. Ansel, T. R. Mempel, H. Lähdesmäki, P. G. Hogan, A. Rao, The transcription factor NFAT promotes exhaustion of activated $CD8^+$ T cells. *Immunity* **42**, 265–278 (2015). doi:10.1016/j.immuni.2015.01.006 Medline

31. L. K. Ward-Kavanagh, W. W. Lin, J. R. Šedý, C. F. Ware, The TNF receptor superfamily in co-stimulating and co-inhibitory responses. *Immunity* **44**, 1005–1019 (2016). doi:10.1016/j.immuni.2016.04.019 Medline

32. P. M. Odorizzi, K. E. Pauken, M. A. Paley, A. Sharpe, E. J. Wherry, Genetic absence of PD-1 promotes accumulation of terminally differentiated exhausted $CD8^+$ T cells. *J. Exp. Med.* **212**, 1125–1137 (2015). doi:10.1084/jem.20142237 Medline

33. O. Boyman, C. Ramsey, D. M. Kim, J. Sprent, C. D. Surh, IL-7/anti-IL-7 mAb complexes restore T cell development and induce homeostatic T cell expansion without lymphopenia. *J. Immunol.* **180**, 7265–7275 (2008). doi:10.4049/jimmunol.180.11.7265 Medline

34. J. N. Blattman, E. J. Wherry, S. J. Ha, R. G. van der Most, R. Ahmed, Impact of epitope escape on PD-1 expression and CD8 T-cell exhaustion during chronic infection. *J. Virol.* **83**, 4386–4394 (2009). doi:10.1128/JVI.02524-08 Medline

35. J. Piper, S. A. Assi, P. Cauchy, C. Ladroue, P. N. Cockerill, C. Bonifer, S. Ott, Wellington-bootstrap: Differential DNase-seq footprinting identifies cell-type determining

transcription factors. *BMC Genomics* **16**, 1000 (2015). doi:10.1186/s12864-015-2081-4 Medline

36. S. Heinz, C. Benner, N. Spann, E. Bertolino, Y. C. Lin, P. Laslo, J. X. Cheng, C. Murre, H. Singh, C. K. Glass, Simple combinations of lineage-determining transcription factors prime cis-regulatory elements required for macrophage and B cell identities. *Mol. Cell* **38**, 576–589 (2010). doi:10.1016/j.molcel.2010.05.004 Medline

37. M. Reich, T. Liefeld, J. Gould, J. Lerner, P. Tamayo, J. P. Mesirov, GenePattern 2.0. *Nat. Genet.* **38**, 500–501 (2006). doi:10.1038/ng0506-500 Medline

38. J. Piper, M. C. Elze, P. Cauchy, P. N. Cockerill, C. Bonifer, S. Ott, Wellington: A novel method for the accurate identification of digital genomic footprints from DNase-seq data. *Nucleic Acids Res.* **41**, e201 (2013). doi:10.1093/nar/gkt850 Medline